



Universiteit  
Leiden  
The Netherlands

## Guiding safe and sustainable technological innovation under uncertainty: a case study of III-V/silicon photovoltaics

Blanco Rocha, C.F.

### Citation

Blanco Rocha, C. F. (2022, September 8). *Guiding safe and sustainable technological innovation under uncertainty: a case study of III-V/silicon photovoltaics*. Retrieved from <https://hdl.handle.net/1887/3455392>

Version: Publisher's Version

License: [Leiden University Non-exclusive license](#)

Downloaded from: <https://hdl.handle.net/1887/3455392>

**Note:** To cite this publication please use the final published version (if applicable).

## **Appendix**

### **Supplementary Information**

## A.1. Supplementary information to Chapter 2

*Table A1-1 Screened and eligible LCA studies of emerging PV technologies*

Year	Authors	Title	PV technology	Eligible	Reason for exclusion
			Organic	Y	
2010	Garcia-Valverde et al. <sup>1</sup>	Life cycle analysis of organic photovoltaic technologies	Silicon Thin Film Silicon Dye-sensitized Organic Thin Film OPV	N N Not LCA Y N	Impact scores not harmonizable Not LCA Integrated on other device Uses data from other studies
2010	Ito et al. <sup>2</sup>	Life-cycle analyses of very-large scale PV systems using six types of PV modules			
2010	Reijnders <sup>3</sup>	Design issues for improved environmental performance of dye-sensitized and organic nanoparticulate solar cells			
2011	Bravi et al. <sup>4</sup>	Life cycle assessment of a micromorph photovoltaic system			
2011	Espinosa et al. <sup>5</sup>	Life-cycle analysis of product integrated polymer solar cells			
2011	Fthenakis & Kim <sup>6</sup>	Photovoltaics: Life-cycle analyses	Silicon Thin Film Silicon Thin Film Chalcogenide	N	
2011	Held & Ig <sup>7</sup>	Update of environmental indicators and energy payback time of CdTe PV systems in Europe	Thin Film	Y	
2011	Kim & Fthenakis <sup>8</sup>	Comparative life-cycle energy payback analysis of multi-junction a-SiGe and nanocrystalline/a-Si modules	Tandem	Y	
2011	Nieves Espinosa et al. <sup>9</sup>	A life cycle analysis of polymer solar cell modules prepared using roll-to-roll methods under ambient conditions	Organic	Y	
2011	Sengül et al. <sup>10</sup>	An environmental impact assessment of quantum dot photovoltaics (QDPV) from raw material acquisition through use	Quantum Dot	Y	
2011	van der Meulen & Alsema <sup>11</sup>	Life-cycle greenhouse gas effects of introducing nano-crystalline materials in thin-film silicon solar cells	Thin Film	Y	
2012	Emmott et al. <sup>12</sup>	Environmental and economic assessment of ITO-free electrodes for organic solar cells	OPV	N	System boundaries not harmonizable Impact scores not harmonizable
2012	Espinosa et al. <sup>13</sup>	Solar cells with one-day energy payback for the factories of the future	OPV	N	Functional unit not harmonizable

2012	Fthenakis <sup>14</sup>	Sustainability metrics for extending thin-film photovoltaics to terawatt levels	Thin Film Chalcogenide Thin Film Silicon	N	Not LCA
2012	Kim et al. <sup>15</sup>	Life Cycle Greenhouse Gas Emissions of Thin-film Photovoltaic Electricity Generation: Systematic Review and Harmonization	Thin Film Chalcogenide Thin Film Silicon	N	Uses data from other studies
2012	Nieves Espinosa et al. <sup>16</sup>	Life cycle assessment of ITO-free flexible polymer solar cells prepared by roll-to-roll coating and printing	Organic OPV	Y	
2012	Raugei et al. <sup>17</sup>	Potential Cd emissions from end-of-life CdTe PV	Thin Film Chalcogenide	N	Not LCA
2012	Yue et al. <sup>18</sup>	Deciphering the uncertainties in life cycle energy and environmental analysis of organic photovoltaics	OPV	N	Uses data from other studies Geographical focus
2012	Zuser & Rechberger <sup>19</sup>	Considerations of resource availability in technology development strategies: The case study of photovoltaics	Thin Film Chalcogenide Thin Film Silicon	N	Not LCA
2013	Eisenberg et al. <sup>20</sup>	Comparative alternative materials assessment to screen toxicity hazards in the life cycle of CIGS thin film photovoltaics	Thin Film Chalcogenide	N	Not LCA
2013	Espinosa et al. <sup>21</sup>	OPV for mobile applications: an evaluation of roll-to-roll processed indium and silver free polymer solar cells through analysis of life cycle, cost and layer quality using inline optical and functional inspection tools	OPV	N	Integrated on other device
2013	Fthenakis et al. <sup>22</sup>	Direct Te Mining: Resource Availability and Impact on Cumulative Energy Demand of CdTe PV Life Cycles	Thin Film Chalcogenide Quantum Dot	N	Uses data from other studies
2013	Kim & Fthenakis <sup>23</sup>	Life Cycle Energy and Climate Change Implications of Nanotechnologies	Tandem	Y	Uses data from other studies
2013	Mohr et al. <sup>24</sup>	Environmental life cycle assessment of roof-integrated flexible amorphous silicon/nanocrystalline silicon solar cell laminate	Dye-sensitized	N	Uses data from other studies Impact scores not harmonizable
2013	Parisi et al. <sup>25</sup>	Development of dye sensitized solar cells: a life cycle perspective for the environmental and market potential assessment of a renewable energy technology			

2014	Collier et al. <sup>26</sup>	Life cycle environmental impacts from CZTS (copper zinc tin sulfide) and Zn3P2 (zinc phosphide) thin film PV (photovoltaic) cells	Thin Film	Y
2014	Espinosa & Krebs <sup>27</sup>	Life cycle analysis of organic tandem solar cells: When are they warranted?	OPV	N Functional unit not harmonizable System boundaries not harmonizable Impact scores not harmonizable
2014	Espinosa et al. <sup>28</sup>	Large scale deployment of polymer solar cells on land, on sea and in the air	OPV	N Functional unit not harmonizable System boundaries not harmonizable Impact scores not harmonizable
2014	Kim et al. <sup>29</sup>	Life cycle assessment of cadmium telluride photovoltaic (CdTe PV) systems	Thin Film	Y
2014	Mann et al. <sup>30</sup>	The energy payback time of advanced crystalline silicon PV modules in 2020: a prospective study	Silicon	N Technology not in development
2014	Parisi et al. <sup>31</sup>	The evolution of the dye sensitized solar cells from Grätzel prototype to up-scaled solar applications: A life cycle assessment approach	Dye-sensitized	Y
2014	Wender et al. <sup>32</sup>	Illustrating Anticipatory Life Cycle Assessment for Emerging Photovoltaic Technologies	Silicon Thin Film Chalcogenide	N Uses data from other studies
2015	Espinosa et al. <sup>33</sup>	Ecodesign of organic photovoltaic modules from Danish and Chinese perspectives	OPV	N Geographical focus
2015	Fabini <sup>34</sup>	Quantifying the Potential for Lead Pollution from Halide Perovskite Photovoltaics	Perovskite	N Not LCA
2015	Gong et al. <sup>35</sup>	Perovskite photovoltaics: life-cycle assessment of energy and environmental impacts	Perovskite	Y
2015	Louwen et al. <sup>36</sup>	Life-cycle greenhouse gas emissions and energy payback time of current and prospective silicon heterojunction solar cell designs	Tandem	Y

2015	Nieves Espinosa et al. <sup>37</sup>	Solution and vapour deposited lead perovskite solar cells: Ecotoxicity from a life cycle assessment perspective	Peroxskite	Y
2015	Prado-Lopez et al. <sup>38</sup>	Tradeoff Evaluation Improves Comparative Life Cycle Assessment: A Photovoltaic Case Study	Silicon Thin Film Silicon Thin Film Chalcogenide	N Uses data from other studies
2015	Scott et al. <sup>39</sup>	Reducing the life cycle environmental impacts of kesterite solar photovoltaics: comparing carbon and molybdenum back contact options	Thin Film Chalcogenide	N System boundaries not harmonizable
2015	Serrano-Lujan et al. <sup>40</sup>	Tin- and Lead-Based Perovskite Solar Cells under Scrutiny: An Environmental Perspective	Peroxskite	Y
2015	Wetzel & Borchers <sup>41</sup>	Update of energy payback time and greenhouse gas emission data for crystalline silicon photovoltaic modules	Silicon	Y
2015	Zhang et al. <sup>42</sup>	Life Cycle Assessment of Titania Perovskite Solar Cell Technology for Sustainable Design and Manufacturing	Peroxskite	Y
2016	Babayigit et al. <sup>43</sup>	Toxicity of organometal halide perovskite solar cells	Peroxskite	N Not LCA
2016	Bergesen & Su <sup>44</sup>	A framework for technological learning in the supply chain: A case study on CdTe photovoltaics	Thin Film Chalcogenide	N Not LCA
2016	Celik et al. <sup>45</sup>	Life Cycle Assessment (LCA) of perovskite PV cells projected from lab to fab	Peroxskite	Y
2016	Chatzisidinis et al. <sup>46</sup>	Ecodesign perspectives of thin-film photovoltaic technologies: A review of life cycle assessment studies	Silicon Thin Film Chalcogenide Tandem III-V	N Uses data from other studies
2016	Hengevoss et al. <sup>47</sup>	Life Cycle Assessment and eco-efficiency of prospective, flexible, tandem organic photovoltaic module	Organic	Y
2016	Kim et al. <sup>48</sup>	Review of life cycle assessment of nanomaterials in photovoltaics	Silicon Thin Film Chalcogenide Quantum Dot	N Uses data from other studies
2016	Leccisi et al. <sup>49</sup>	The Energy and Environmental Performance of Ground-Mounted Photovoltaic Systems—A Timely Update	Thin Film	Y

2016	Scott et al. <sup>50</sup>	Can Carbon Nanomaterials Improve CZTS Photovoltaic Devices? Evaluation of Performance and Impacts Using Integrated Life-Cycle Assessment and Decision Analysis	Thin Film Chalcogenide	N	System boundaries not harmonizable
2016	Tsang et al. <sup>51</sup>	A comparative human health, ecotoxicity, and product environmental assessment on the production of organic and silicon solar cells	Organic OPV	Y	
2016	Tsang et al. <sup>52</sup>	Life-cycle assessment of cradle-to-grave opportunities and environmental impacts of organic photovoltaic solar panels compared to conventional technologies	Tandem OPV	N	Uses data from other studies
2017	Celik et al. <sup>53</sup>	Environmental analysis of perovskites and other relevant solar cell technologies in a tandem configuration	Organic OPV	Y	
2017	Celik et al. <sup>54</sup>	Environmental Impacts from Photovoltaic Solar Cells Made with Single Walled Carbon Nanotubes	Perovskite	N	Integrated on other device
2017	dos Reis Benatto et al. <sup>55</sup>	Life-Cycle Assessment of Solar Charger with Integrated Organic Photovoltaics	Perovskite	N	System boundaries not harmonizable
2017	Hauck et al. <sup>56</sup>	Environmental benefits of reduced electricity use exceed impacts from lead use for perovskite based tandem solar cell	Tandem	Y	
2017	Itten & Stucki <sup>57</sup>	Highly Efficient 3rd Generation Multi-Junction Solar Cells Using Silicon Heterojunction and Perovskite Tandem: Prospective Life Cycle Environmental Impacts	Silicon Thin Film Silicon	N	Geographical focus
2017	Khaenson et al. <sup>58</sup>	A comparison of the environmental impact of solar power generation using multicrystalline silicon and thin film of amorphous silicon solar cells: case study in Thailand	Tandem	Y	
2017	Lunardi et al. <sup>59</sup>	A life cycle assessment of perovskite/silicon tandem solar cells	Silicon Thin Film Chalcogenide	N	Impact scores not harmonizable
2017	Vellini et al. <sup>60</sup>	Environmental impacts of PV technology throughout the life cycle: Importance of the end-of-life management for Si-panels and CdTe-panels	Perovskite	Y	
2017	Zhang et al. <sup>61</sup>	Comparison of life cycle environmental impacts of different perovskite solar cell systems	Perovskite	Y	
2018	Alberola-Borràs et al. <sup>62</sup>	Perovskite Photovoltaic Modules: Life Cycle Assessment of Pre-industrial Production Process	Perovskite	Y	
2018	Alberola-Borràs et al. <sup>63</sup>	Relative impacts of methylammonium lead triiodide perovskite solar cells based on life cycle assessment	Perovskite	Y	

2018	Alberola-Borràs et al. <sup>64</sup>	Evaluation of multiple cation/anion perovskite solar cells through life cycle assessment	Perovskite	N	Functional unit not harmonizable Uses data from other studies
2018	Amarakoon et al. <sup>65</sup>	Life cycle assessment of photovoltaic manufacturing consortium (PVMC) copper indium gallium (di)selenide (CIGS) modules	Thin Film	Y	
2018	Celik et al. <sup>66</sup>	Energy Payback Time (EPBT) and Energy Return on Energy Invested (EROI) of Perovskite Tandem Photovoltaic Solar Cells	Perovskite	Y	
2018	Celik et al. <sup>67</sup>	Life cycle analysis of metals in emerging photovoltaic (PV) technologies: A modeling approach to estimate use phase leaching	Thin Film Chalcogenide Perovskite	N	System boundaries not harmonizable
2018	Lunardi et al. <sup>68</sup>	A comparative life cycle assessment of chalcogenide/Si tandem solar modules	Tandem	Y	
2018	Lunardi et al. <sup>69</sup>	Life cycle assessment on PERC solar modules	Silicon	Y	
2018	Mokhtarimehr et al. <sup>70</sup>	Environmental assessment of vacuum and non-vacuum techniques for the fabrication of Cu2ZnSnS4 thin film photovoltaic cells	Thin Film	Y	
2018	Moore et al. <sup>71</sup>	Portfolio Optimization of Nanomaterial Use in Clean Energy Technologies	OPV	N	Not LCA
2018	Munshi et al. <sup>72</sup>	Thin-film CdTe photovoltaics – The technology for utility scale sustainable energy generation	Thin Film	N	Not LCA Uses data from other studies
2018	Pallas et tal. <sup>73</sup>	Green and Clean: Reviewing the Justification of Claims for Nanomaterials from a Sustainability Point of View	Perovskite Thin Film Silicon Tandem OPV	N	Uses data from other studies
2018	Ravikumar et al. <sup>74</sup>	Novel Method of Sensitivity Analysis Improves the Prioritization of Research in Anticipatory Life Cycle Assessment of Emerging Technologies	Dye-sensitized Thin Film Chalcogenide Thin Film Ribbon	N	Uses data from other studies

2018	Salim et al. <sup>75</sup>	<i>A Fuzzy Based Model for Standardized Sustainability Assessment of Photovoltaic Cells</i>	Silicon Thin Film Chalcogenide Thin Film Silicon Tandem III-V	Thin Film	N	Uses data from other studies
2018	Sinha & Wade <sup>76</sup>	<i>Addressing Hotspots in the Product Environmental Footprint of CdTe Photovoltaics</i>	Silicon Thin Film Chalcogenide Silicon	Thin Film	Y	
2018	Soares et al. <sup>77</sup>	<i>LCA study of photovoltaic systems based on different technologies</i>	Silicon Thin Film Chalcogenide Silicon	Thin Film	N	Uses data from other studies
2018	Stamford & Azapagic <sup>78</sup>	<i>Environmental Impacts of Photovoltaics: The Effects of Technological Improvements and Transfer of Manufacturing from Europe to China</i>	Assessing the photovoltaic technology landscape: efficiency and energy return on investment (EROI)	Thin Film Chalcogenide OPV	N	Not LCA Uses data from other studies
2018	Zhou et al. <sup>79</sup>		Comparative evaluation of lead emissions and toxicity potential in the life cycle of lead halide perovskite photovoltaics	Perovskite	N	System boundaries not harmonizable
2019	Billen et al. <sup>80</sup>		Life cycle assessment of emerging technologies at the lab scale: The case of nanowire-based solar cells	Tandem	Y	
2019	Pallas et al. <sup>81</sup>		Environmental impacts of III-V/silicon photovoltaics: life-cycle assessment and guidance for sustainable manufacturing	Tandem	Y	
2020	Blanco et al. <sup>82</sup>					

Table A.1-2 Conversion factors for LCA impact category indicators

LCIA method	Version	Impact category	Indicator unit	Conversion factor	Resulting ILCD indicator unit
CED		Cumulative Energy Demand	CED	1	MJ
CML	2014	Abiotic Depletion Potential	CML-ADP	1	kg Sb eq
CML	2014	Abiotic Depletion Potential	CML-ADPf		MJ
CML	2014	Acidification potential	CML-AP	1.19	kg SO2 eq
CML	2014	Climate change	CML-CC	1	kg CO2 eq
CML	2014	Eutrophication potential	CML-EP	0.28	kg PO4 eq
CML	2014	Freshwater aquatic ecotoxicity potential	CML-FAETP	42.15	kg 1,4 DB eq
CML	2014	Human toxicity potential	CML-HTP		kg 1,4 DB eq
CML	2014	Land Use	CML-LU		m2.y
CML	2014	Marine aquatic ecotoxicity potential	CML-MAETP		kg 1,4 DB eq
CML	2014	Ozone depletion potential	CML-ODP	1	kg CFC-11 eq
CML	2014	Photochemical oxidation potential	CML-POCP	10.86	kg C2H4 eq
CML	2014	Terrestrial ecotoxicity potential	CML-TETP		kg 1,4 DB eq
CML	2014	Water depletion potential	CML-WDP	1	m3 water
EPBT		Energy payback time	EPBT	1	years
ILCD	2011	Resource use, minerals and metals	ILCD-ADP	1	kg Sb eq
ILCD	2011	Acidification	ILCD-AP	1	molc H+ eq
ILCD	2011	Climate change	ILCD-CC	1	kg CO2 eq
ILCD	2011	Freshwater ecotoxicity	ILCD-FET	1	CTUe
ILCD	2011	Freshwater eutrophication	ILCD-FEU	1	kg P eq
ILCD	2011	Human toxicity potential - cancer effects	ILCD-HT_CE	1	CTUh,c
ILCD	2011	Human toxicity potential - non cancer effects	ILCD-HT_NCE	1	CTUh,nc
ILCD	2011	Ionizing radiation	ILCD-IR	1	kBq U235 eq
ILCD	2011	Marine eutrophication	ILCD-MEUP	1	kg N
ILCD	2011	Ozone depletion	ILCD-ODP	1	kg CFC-11 eq
ILCD	2011	Respiratory inorganics	ILCD-PM	1	kg PM2.5 eq
ILCD	2011	Photochemical ozone formation	ILCD-POCP	1	kg NMVOC eq
ILCD	2011	Terrestrial eutrophication	ILCD-TEUP	1	mol N eq
ILCD	2011	Water resource depletion	ILCD-WRD	1	m3 water
Impact 2002+	2011	Aquatic acidification	IM2-AC	1.21	kg SO2 eq
Impact 2002+	2011	Climate change	IM2-CC	1	kg CO2 eq

Impact 2002+	2011	Ozone layer depletion	IM2-OD	1	kg CFC-11 eq
Impact 2002+	2011	Terrestrial ecotoxicity	IM2-TE		kg TEG eq
Recipe	2008	Agricultural land occupation	R8-ALO(H)		m2.y
Recipe	2008	Climate change (H)	R8-CC(H)	1	kg CO2 eq
Recipe	2008	Fossil depletion	R8-FD(H)		MJ
Recipe	2008	Freshwater ecotoxicity (H)	R8-FET(H)	544.78	kg 1,4 DB eq
Recipe	2008	Freshwater eutrophication potential	R8-FEU(H)	1	kg P eq
Recipe	2008	Human toxicity (H)	R8-HT(H)		kg 1,4 DB eq
Recipe	2008	Ionising radiation	R8-IR(H)	1	kBq U235
Recipe	2008	Marine ecotoxicity (H)	R8-MET(H)		kg 1,4 DB eq
Recipe	2008	Marine eutrophication potential	R8-MEU(H)	2.76	kg N eq
Recipe	2008	Mineral resource depletion	R8-MRD(H)	1.66E-06	kg Fe eq
Recipe	2008	Natural land transformation	R8-NLT(H)		m2
Recipe	2008	Ozone depletion (H)	R8-OD(H)	1	kg CFC-11 eq
Recipe	2008	Particulate matter	R8-PMF(H)	0.28	kg PM10 eq
Recipe	2008	Photochemical oxidant formation	R8-POF(H)	1	kg NMVOC eq
Recipe	2008	Terrestrial acidification	R8-TA(H)	1.32	kg SO2 eq
Recipe	2008	Terrestrial ecotoxicity (H)	R8-TET(H)		kg 1,4 DB eq
Recipe	2008	Urban land occupation	R8-ULO(H)		m2.y
Recipe	2008	Water depletion	R8-WD(H)	1	m3 water
TRACI v2.1		Acidification	TR-AC	1.21	kg SO2 eq
TRACI v2.1		Climate change	TR-CC	1	kg CO2 eq
TRACI v2.1		Ecotoxicity	TR-ET	1	CTUe
TRACI v2.1		Eutrophication	TR-EU	0.13	kg N

Table A.1-3 Pearson's correlations for impact as a function of year for each cell type

Impact Category	Cell type	Pearson's Correlation (Impact = f(Year))	Number of observations
CTUe	Organic	-0.35	7
CTUe	Perovskite	-0.20	19
CTUe	Silicon	NA	10
CTUe	Tandem	0.31	20
CTUe	Thin Film (Chalcogenide)	-0.84	6
CTUh,c	Organic	NA	2
CTUh,c	Perovskite	-0.07	10
CTUh,c	Silicon	NA	6

CTUh,c	Tandem	-0.04	17
CTUh,c	Thin Film (Chalcogenide)	-0.13	4
CTUh,nc	Organic	NA	2
CTUh,nc	Perovskite	0.01	19
CTUh,nc	Silicon	NA	6
CTUh,nc	Tandem	-0.14	17
CTUh,nc	Thin Film (Chalcogenide)	-0.12	4
kBq U235 eq	Organic	NA	3
kBq U235 eq	Perovskite	0.82	4
kBq U235 eq	Tandem	0.66	5
kBq U235 eq	Thin Film (Chalcogenide)	1.00	2
kg CFC-11 eq	Organic	0.59	5
kg CFC-11 eq	Perovskite	0.15	9
kg CFC-11 eq	Silicon	NA	6
kg CFC-11 eq	Tandem	-0.56	11
kg CFC-11 eq	Thin Film (Chalcogenide)	-0.44	9
kg CO2 eq	Dye-sensitized	NA	3
kg CO2 eq	Organic	-0.28	10
kg CO2 eq	Perovskite	-0.07	21
kg CO2 eq	Quantum Dot	NA	1
kg CO2 eq	Silicon	-0.27	14
kg CO2 eq	Tandem	0.05	28
kg CO2 eq	Thin Film (Chalcogenide)	-0.33	13
kg CO2 eq	Thin Film (Si)	-0.84	5
kg N eq	Organic	NA	3
kg N eq	Perovskite	0.94	6
kg N eq	Tandem	0.93	5
kg NMVOC eq	Organic	0.54	5
kg NMVOC eq	Perovskite	0.44	9
kg NMVOC eq	Silicon	NA	4
kg NMVOC eq	Tandem	0.64	11
kg NMVOC eq	Thin Film (Chalcogenide)	-0.95	5
kg P eq	Organic	0.49	5
kg P eq	Perovskite	0.37	15
kg P eq	Silicon	NA	10
kg P eq	Tandem	0.34	20
kg P eq	Thin Film (Chalcogenide)	0.68	5
kg PM2.5 eq	Organic	0.51	5
kg PM2.5 eq	Perovskite	0.26	9
kg PM2.5 eq	Tandem	0.59	9
kg PM2.5 eq	Thin Film (Chalcogenide)	0.23	4
kg Sb eq	Organic	NA	3
kg Sb eq	Perovskite	-0.22	16
kg Sb eq	Silicon	NA	10

kg Sb eq	Tandem	0.78	14
kg Sb eq	Thin Film (Chalcogenide)	0.53	3
m3 water	Organic	NA	3
m3 water	Perovskite	-0.92	7
m3 water	Tandem	-1.00	3
m3 water	Thin Film (Chalcogenide)	NA	2
MJ	Dye-sensitized	NA	3
MJ	Organic	-0.84	7
MJ	Perovskite	-0.20	15
MJ	Quantum Dot	NA	1
MJ	Silicon	NA	2
MJ	Tandem	NA	2
MJ	Thin Film (Chalcogenide)	0.60	5
MJ	Thin Film (Si)	NA	1
mol N eq	Tandem	0.81	4
mol N eq	Thin Film (Chalcogenide)	NA	1
molc H+ eq	Organic	0.52	5
molc H+ eq	Perovskite	-0.18	12
molc H+ eq	Quantum Dot	NA	1
molc H+ eq	Silicon	NA	6
molc H+ eq	Tandem	0.54	11
molc H+ eq	Thin Film (Chalcogenide)	0.31	10

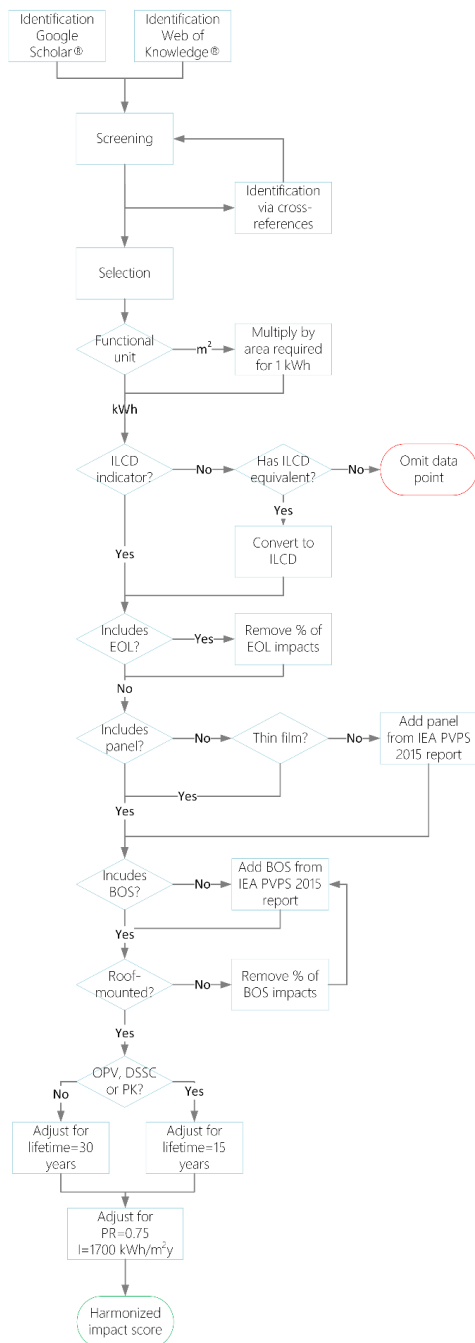


Figure A.1-1 Identification, screening, selection and harmonization procedure flowchart

Source	SMD (95% CI)
<b>EFFICIENCY = Low</b>	
a-Si	-0.72 [-2.15; 0.70]
CZTS	-1.14 [-2.34; 0.06]
micro-Si	-0.63 [-1.81; 0.55]
PCBM:P3HT	-1.06 [-1.85; -0.27]
Ru(II) dye	-0.81 [-1.99; 0.38]
SWCNT	-0.58 [-2.00; 0.85]
Total	-0.88 [-1.12; -0.64]
Heterogeneity: $\chi^2_5 = 0.79$ ( $P = .98$ ), $I^2 = 0\%$	

**EFFICIENCY = Mid**

CdTe	-1.33 [-2.30; -0.36]
CIGS	-1.37 [-2.43; -0.30]
Lead halide	1.32 [ 0.72; 1.91]
multi-Si	-0.85 [-1.90; 0.19]
PK/Si	2.47 [ 1.59; 3.35]
SHJ	-1.04 [-1.83; -0.25]
single-Si	-0.82 [-1.53; -0.11]
TF-Ch/PK	-1.07 [-2.51; 0.37]
TF-Ch/Si	-0.98 [-2.17; 0.21]
Tin halide	12.44 [ 9.33; 15.54]
Total	0.74 [-2.17; 3.64]

Heterogeneity:  $\chi^2_9 = 143.41$  ( $P < .01$ ),  $I^2 = 94\%$

**EFFICIENCY = High**

III-V/Si	2.91 [ 1.71; 4.12]
Total	2.91 [ 1.71; 4.12]
Heterogeneity: not applicable	

Total 0.27 [-1.34; 1.87]

Prediction interval [-6.50; 7.03]

Heterogeneity:  $\chi^2_{16} = 180.08$  ( $P < .01$ ),  $I^2 = 91\%$

Residual heterogeneity:  $\chi^2_{14} = 144.20$  ( $P < .01$ ),  $I^2 = 90\%$

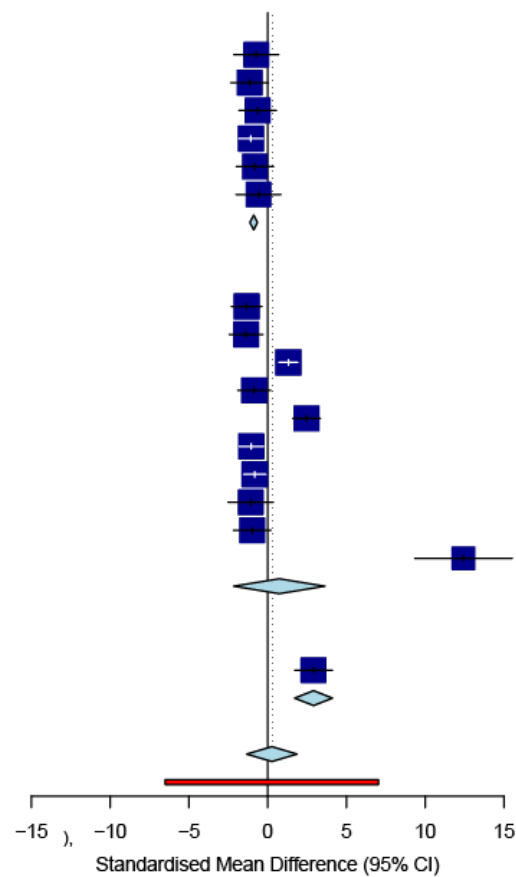


Figure A.1-1 Random effect model results sub-grouped by cell conversion efficiencies.

## A.2. Supplementary Information to Chapter 3

### A.2.1. System flowcharts and boundaries

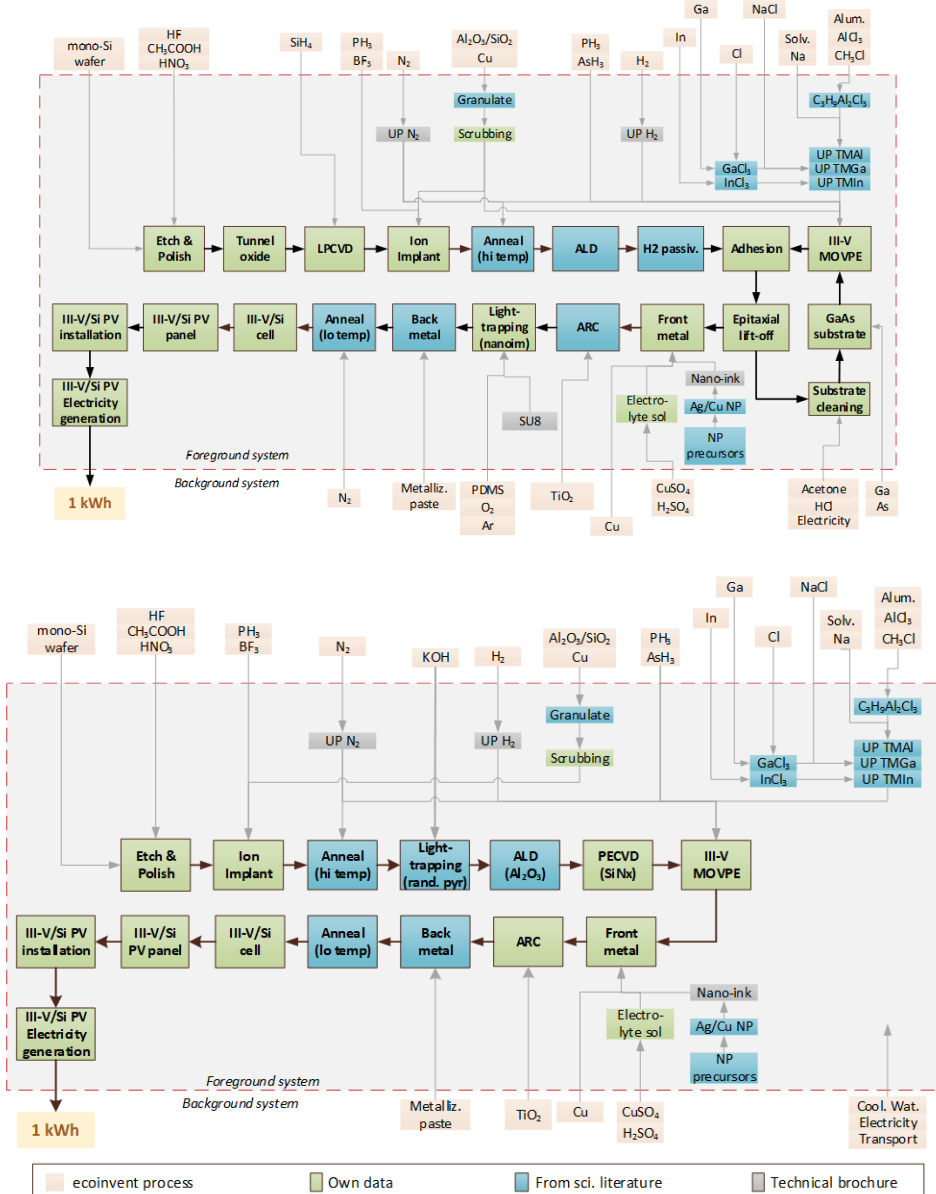


Figure A.2-1 System flowchart for Concept A (direct growth, bottom) and Concept B (bonding, top). UP = Ultrapure

## A.2.2. Life-cycle inventories: process descriptions and input/output data

### A.2.2.1. Overview and general assumptions

Most of the foreground processes are sensitive to the wafer area that can be processed per run since materials and energy consumption scale proportionally with the treatable wafer area. We based our models on the use of a large MOVPE reactor prototype designed by AIXTRON, which can handle a run of 31 round 4-inch wafers. We assumed that all other processing steps would handle wafers of the same area.

We also note that some lab-based processes described below have been modelled considering only process inputs, while waste emissions have not been fully characterized. The characterization of waste streams and emissions is more relevant in industrial-scale implementations where recycling and reuse take a central role and differ significantly from waste management in a lab environment. However, based on extrapolation from similar processes, it is likely that these emissions would only have relatively minor contributions to the life cycle impacts of the electricity generation process.

### A.2.2.2. Silicon wafer preparation

Table A.2-1 Process inputs and outputs for silicon wafer preparation

Input	Flow type	Quantity	Data source
CZ single-Si wafer	Eco	100 units	TopSil, personal communication
HF	Eco	0.3 L	TopSil, personal communication
HNO <sub>3</sub>	Eco	1.6 L	TopSil, personal communication
HC <sub>2</sub> H <sub>2</sub> O <sub>2</sub>	Eco	0.1 L	TopSil, personal communication
Treatment of wastewater from PV cell production	Eco	2 L	TopSil, personal communication
Output	Flow type	Quantity	Data source
Polished Si wafer	Eco	100 units	TopSil, personal communication

### A.2.2.3. Ion implantation (*p-n* junction)

Table A.2-2. Process inputs and outputs for ion implantation

Input	Flow type	Quantity	Data source
Phosphine (PH <sub>3</sub> )	Eco	3.4 g	Fraunhofer, personal communication
Boron trifluoride (BF <sub>3</sub> )	Eco	3.4 g	Fraunhofer, personal communication
Ultrapure nitrogen (N <sub>2</sub> )	Eco	14 m <sup>3</sup>	Fraunhofer, personal communication
Cooling water	Eco	5 m <sup>3</sup>	Fraunhofer, personal communication
Electricity, high voltage	Eco	100 kWh	Fraunhofer, personal communication
Compressed air	Eco	15 m <sup>3</sup>	Fraunhofer, personal communication
Hazardous waste incineration	Eco	0.009 kg	Calculated
Output	Flow type	Quantity	Data source
Doped wafer area (3400 wafers)	Eco	26.69 m <sup>2</sup>	Fraunhofer, personal communication

#### A.2.2.4. Tube furnace annealing – high temperature

We assumed the use of a 4.2kW power furnace which can handle 100 wafers per batch. The wafers cannot be inserted at 1000°C; this must be done at <400°C, and then the temperature is ramped up at a rate of 10°C per minute. The annealing time is 1 hour at 1000°C and the temperature is then ramped down for removal of the wafers. We assume a worst-case scenario where the furnace operates at full power during ramp up and processing time. We assume no power is consumed during ramp-down. Annealing is conducted in an inert environment of ultrapure nitrogen, which flows at a rate of 30 SLM (standard litres per minute) during insertion and removal, and 15 SLM during annealing.

*Table A.2-3. Process inputs and outputs for high temperature tube furnace annealing*

Flow type	Flow type	Quantity	Data source
Ultrapure nitrogen	Eco	0.9 m <sup>3</sup>	AZUR, personal communication
Electricity	Eco	10.668 kWh	Calculated
Output	Flow type	Quantity	Data source
Annealing of 1 m <sup>2</sup> of cell	Eco	1 unit	Calculated

#### A.2.2.5. Atomic layer deposition (ALD)

This step considers the deposition of a 10nm film of Al<sub>2</sub>O<sub>3</sub> on the rear side. Process data for this step is based on Louwen et al.<sup>83</sup>, who reviewed various specifications and found average electricity use to be 0.29 kWh/m<sup>2</sup>, with values ranging 0.15 to 0.51 kWh/m<sup>2</sup> (-48% to +76%). No materials input data and output data were available for this step.

#### A.2.2.6. Back-side passivation

Back-side passivation is conducted by plasma-enhanced chemical vapour deposition (PECVD) of a SiNx layer.

*Table A.2-4. Energy and material inputs and outputs for PECVD back-side passivation*

Input	Flow type	Quantity	Data source
Electricity	Eco	39,93 Wh	Fraunhofer, personal communication
Cooling water	Eco	5,27 L	Fraunhofer, personal communication
Nitrogen	Eco	12,57 L	Fraunhofer, personal communication
Compressed dry air	Eco	5,02 L	Fraunhofer, personal communication
Silane (SiH <sub>4</sub> )	Eco	0,03 L	Fraunhofer, personal communication
NH <sub>3</sub>	Eco	0,06 L	Fraunhofer, personal communication
Output	Flow type	Quantity	Data source
Back-side passivation of 1 cell	Eco	1 unit	Fraunhofer, personal communication

### A.2.2.7. III-V Metalorganic Vapor Phase Epitaxy (MOVPE)

Table A.2-5. Process inputs and outputs for MOVPE III-V direct growth

Input	Flow type	Quantity	Data source
TMGa	Eco	11.48 g	Aixtron, personal communication
TMIn	Eco	0.1 g	Aixtron, personal communication
TMAI	Eco	0.17 g	Aixtron, personal communication
AsH3	Eco	11.76 g	Aixtron, personal communication
PH3	Eco	17.84 g	Aixtron, personal communication
H2	Eco	3.34 m3	Aixtron, personal communication
N2	Eco	3.44 m3	Aixtron, personal communication
Cooling water	Eco	27.51 m3	Aixtron, personal communication
Electricity	Eco	105.06 kWh	Aixtron, personal communication
Hazardous waste treatment	Eco	0.035 kg	Calculated
Output	Flow type	Quantity	Data source
III-V layer area	Eco	2905 cm <sup>2</sup>	Aixtron, personal communication

### A.2.2.8. Front metal contacts

We based our model on a “seed and plate” metallization technique, which involves nanoink printing of a seed layer of fingers, then electroplating to increase the thickness of the fingers. Conventional screen-printing methods are considered for 3 busbars that cross the fingers.

#### A.2.2.8.1. Seed layer (nano) inkjet printing

Materials: The pattern to be printed on the cells for the seed layer consists of 6 fingers 2 mm wide, 75 mm long and 0.1 µm thick (height) on average. The total quantity of nanoink required is calculated by the total volume of this pattern multiplied by the density of the nanoink (reported by the manufacturer). To this quantity, we added 10% to account for ink that remains in the filter and is discarded as hazardous waste. Therefore, we have the following inputs, per cell:

$$\# \text{fingers} \quad \text{Finger width} \quad \text{Finger length} \quad \text{Finger thickness} \quad \text{Ink density} \quad \text{Loss factor} \quad (\text{Eq. A.2-1})$$

$$6 \cdot \left( 2 \text{ mm} \cdot \frac{1 \text{ m}}{1E3 \text{ mm}} \right) \cdot \left( 75 \text{ mm} \cdot \frac{1 \text{ m}}{1E3 \text{ mm}} \right) \cdot \left( 0.1 \mu\text{m} \cdot \frac{1 \text{ m}}{1E6 \mu\text{m}} \right) \cdot \frac{1.27E3 \text{ kg}}{\text{m}^3} \cdot 110\% = 1.25E - 7 \text{ kg Cu ink}$$

Printer electricity. A sample tested at Joanneum Research Center facilities was approximately 10 cm. long and took 5 minutes to print, with only 2 nozzles in use out of a total possible of 210. We estimated the printing speed as:

$$\frac{10 \text{ cm}}{5 \text{ min}} \cdot \frac{210 \text{ nozzles}}{2 \text{ nozzles}} \cdot \frac{60 \text{ min}}{1 \text{ h}} \cdot \frac{1 \text{ m}}{100 \text{ cm}} = \frac{126 \text{ m}}{\text{h}} \quad (\text{Eq. A.2-2})$$

The total length of the 6 printed fingers is 0.45 m, and the printer has a maximum power rating of 1kW. We assume it operates at 75% power on average. To calculate electricity consumption of the printing process (per cell) we have:

$$\frac{0.45 \text{ m}}{\text{cell}} \cdot \frac{1 \text{ h}}{126 \text{ m}} \cdot 1 \text{ kW} \cdot 75\% = \frac{0.027 \text{ kWh}}{\text{cell}} \quad (\text{Eq. A.2-3})$$

#### A.2.2.8.2. Seed layer sintering: laser

Laser electricity: The length of the pattern that has to be sintered is calculated from the data in the previous section (0.45 m). We used a laser scan speed of 0.01 m/s, and the optical power delivered by the laser is 1.4 W. The wall-plug to optical efficiency of YAG type lasers is typically around 25%<sup>84</sup>, so we estimate the electricity consumption for laser sintering as:

$$\frac{0.45 \text{ m}}{\text{cell}} \cdot \frac{s}{0.01 \text{ m}} \cdot \frac{1 \text{ h}}{3600 \text{ s}} \cdot 1.4 \text{ E} - 3 \text{ kW} \cdot \frac{1}{25\%} = \frac{5.6E - 5 \text{ kWh}}{\text{cell}} \quad (\text{Eq. A.2-4})$$

Materials: Laser-sintering of both Cu and Ag ink is done in open air.

Table A.2-6. Process inputs and outputs for seed-layer inkjet printing

Input	Flow type	Quantity	Data source
Cu nanoink	Eco	1.25E-7 kg	Joanneum, personal communication
Electricity	Eco	0.0271 kWh	Joanneum, personal communication
Output	Flow type	Quantity	Data source
Finger seed layers for 1 cell	Eco	1 unit	Joanneum, personal communication

#### A.2.2.8.3. Seed layer sintering: chemical (Cu ink only)

Sintering of Cu ink requires a reducing environment, while Ag ink can be sintered in open air. For the Cu ink, a sintering test was conducted at Joanneum Research Center facilities, where for a 1cm<sup>2</sup> sample 5 mL of ethanol (3.95 g @ 789g/L), 50 mL formic acid, and 70 L of ultrapure nitrogen were required.

#### A.2.2.8.4. Fingers electroplating

Electroplating consists of submerging the cell with the seed pattern in an electrolyte bath, where the patterned cell will serve as an ion-receiving cathode and a copper in the solution will serve as an anode. For copper, the electrolyte solution consists of a mix of cupric sulphate and sulphuric acid. Driving an electric current through the solution will force the metallic ions from the cathode to deposit on the seed pattern until the desired geometry is obtained.

Electricity: A conventional electroplating setup is used, where 10 mA of applied current with an average voltage of 0.5 V provides 250 nm of plating per minute. The electrical power can be calculated from the current and voltage:

$$P = I \cdot V = \left(10 \text{ mA} \cdot \frac{1 \text{ A}}{1000 \text{ mA}}\right) \cdot (0.5 \text{ V}) = 5E - 3 \text{ W} = 5E - 6 \text{ kW} \quad (\text{Eq. A.2-5})$$

The amount of electricity consumed is calculated by multiplying the power by the time required to plate the desired finger thickness of 12.5µm.

$$\frac{5E - 6 \text{ kW}}{\text{cells}} \cdot \frac{1 \text{ min}}{0.25 \mu\text{m}} \cdot 12.5 \mu\text{m} \cdot \frac{1 \text{ h}}{60 \text{ min}} = \frac{4.16E - 6 \text{ kWh}}{\text{cell}} \quad (\text{Eq. A.2-6})$$

Materials: Pure metal anodes donate the ions that ultimately deposit on the pattern (cathode). The ions are first passed from the electrolyte solution to the cathode, and are then replenished from the anode to the solution. Therefore, the anode is sacrificed according to the amount of metal deposited in the cell, and we assume 10% losses.

(Eq. A.2-7)

$$Cu: 6 \cdot \left(2 \text{ mm} \cdot \frac{1 \text{ m}}{1E3 \text{ mm}}\right) \cdot \left(75 \text{ mm} \cdot \frac{1 \text{ m}}{1E3 \text{ mm}}\right) \cdot \left(12.4 \mu\text{m} \cdot \frac{1 \text{ m}}{1E6 \mu\text{m}}\right) \cdot \frac{8.96E3 \text{ kg}}{\text{m}^3} \cdot 110\% = 1.09E - 4 \text{ kg Cu}$$

We consider a standard cupric sulphate electrolyte solution that consists of 200 g cupric sulphate and 25 mL sulphuric acid in sufficient deionized water to prepare 1 L of electrolyte solution. This amount of solution is used for electroplating on one cell; however, we consider that it can be used for the production of 10-100 wafers based on lab experience, and test the sensitivity of this parameter.

Table A.2-7. Energy and material inputs and outputs for electroplating of fingers

Input	Flow type	Quantity	Data source
Copper	Eco	1.09E-4 kg	Joanneum, personal communication
Electricity	Eco	4.16E-6 kWh	Joanneum, personal communication
Electrolyte solution	Eco	0.1 L	Joanneum, personal communication
Output	Flow type	Quantity	Data source
Electroplating of 1 cell	Eco	1 unit	Joanneum, personal communication

#### A.2.2.8.5. Busbars screen printing

Screen printing electricity: We use data from a screen printer running a squeegee motor with a power of 1.16 kW. The printer can process a sheet of 400x400mm in 30 seconds.

$$\frac{1 \text{ sheet}}{4 \text{ cells}} \cdot 1.16 \text{ kW} \cdot 30 \text{ s} \cdot \frac{1 \text{ h}}{3600 \text{ s}} = \frac{2.41E - 3 \text{ kWh}}{\text{cell}} \quad (\text{Eq. A.2-8})$$

Curating electricity: Cu busbars are grown over the Cu fingers by screen-printing. However, instead of co-firing, the Cu busbars are curated at lower temperature (250°C) in an atmosphere of pure nitrogen<sup>85</sup>. This is done in a furnace that has a power rating of 3.4 kW and can process 1000 cells per batch, for a curating time of 10 minutes.

$$\frac{3.4 \text{ kW}}{1000 \text{ cells}} \cdot 10 \text{ min} \cdot \frac{1 \text{ h}}{60 \text{ min}} = \frac{5.67E - 4 \text{ kWh}}{\text{cell}} \quad (\text{Eq. A.2-9})$$

Materials: We consider 3 busbars, 1 mm wide, 156 mm long and 13.5 μm thick on average. We assume 10% losses from the paste during screen-printing. Per cell, we have:

(Eq. A.2-10)

$$3 \cdot \left(1 \text{ mm} \cdot \frac{1 \text{ m}}{1E3 \text{ mm}}\right) \cdot \left(156 \text{ mm} \cdot \frac{1 \text{ m}}{1E3 \text{ mm}}\right) \cdot \left(13.5 \mu\text{m} \cdot \frac{1 \text{ m}}{1E6 \mu\text{m}}\right) \cdot \frac{8.96E3 \text{ kg}}{\text{m}^3} \cdot 110\% = 6.23E - 5 \text{ kg Cu}$$

Table A.2-8. Energy and material inputs and outputs for screen printing of busbars

Input	Flow type	Quantity	Data source
Copper	Eco	6.23E-5 kg	Joanneum, personal communication
Electricity	Eco	3E-3 kWh	Joanneum, personal communication
Output	Flow type	Quantity	Data source
Screen printing of 1 cell	Eco	1 unit	Joanneum, personal communication

#### A.2.2.9. Rear-side metal contacts

Data for the rear-side metal contacts are taken from the inventories for existing single-Si PV cells (ecoinvent v3.4)<sup>86</sup>.

#### A.2.2.10. Tube furnace annealing - low temperature

The data for this process was calculated as for the high temperature annealing in section 2.4; however we discard ramp up energy and gas flow requirements, since the cells can be inserted and removed at this lower process temperature (<400°C).

#### A.2.2.11. Carrier gases

##### A.2.2.11.1. Ultrapure hydrogen

Two alternatives are considered for the supply of ultrahigh purity hydrogen: off-site source (commercially available hydrogen produced from Steam Methane Reforming) and on-site generation with a proton exchange membrane (PEM) system. In both alternatives, additional purification with a two-step adsorber/getter is considered.

*Off-site generation: Commercial H<sub>2</sub> gas + adsorber/getter.* Commercial production of hydrogen gas is modelled based on the steam methane reforming process (SMR), which accounts for over 90% of the world production. This production method was modelled in an LCA study by NREL<sup>87</sup> and more recently by other authors<sup>88,89</sup>. We use the process data reported by Cetinkaya et al.<sup>89</sup>, which is in close accordance with figures reported by Mehmeti et al.<sup>88</sup>. The inputs required for generating electricity that is consumed in the SMR process are also included in the inventory.

Table A.2-9. Process inputs and outputs for production of hydrogen via steam methane reforming

Input	Flow type	Quantity	Data source
Concrete	Eco	5.26E-06 m <sup>3</sup>	Cetinkaya et al. <sup>89</sup>
cast iron	Eco	0.049 g	Cetinkaya et al. <sup>89</sup>
steel, low-alloyed	Eco	4.029 g	Cetinkaya et al. <sup>89</sup>
aluminium, cast alloy	Eco	0.033 g	Cetinkaya et al. <sup>89</sup>
water, deionised	Eco	19,776.2 g	Cetinkaya et al. <sup>89</sup>
natural gas; 44.1 MJ/kg	Env	165 MJ	Cetinkaya et al. <sup>89</sup>
Coal, hard, unspecify., in ground	Env	132.49 g	Cetinkaya et al. <sup>89</sup>
Oil, crude, in ground	Env	8.76 g	Cetinkaya et al. <sup>89</sup>

Output	Flow type	Quantity	Data source
Hydrogen	Eco	1 kg	Cetinkaya et al. <sup>89</sup>

The purifier (adsorber + getter) commercialized by SAES Gas handles a flow of 100 Nm<sup>3</sup>/h at an average power consumption of 26kW, therefore 0.26kWh/Nm<sup>3</sup>. It also consumes 60 L/min of cooling water, therefore 0.036 m<sup>3</sup> water/Nm<sup>3</sup>. In this case we include transportation from SMR plant to consumer, using the same values as for liquid hydrogen specified in EcoInvent v3.4.

Table A.2-10. Process inputs and outputs for purification of hydrogen

Input	Flow type	Quantity	Data source
Hydrogen	Eco	0.08988 kg	SAES product spec sheet
Electricity	Eco	0.26 kWh	SAES product spec sheet
Cooling water	Eco	0.036 m <sup>3</sup>	SAES product spec sheet
transport, freight train	Eco	0.0004 t*km	EcoInvent v3.4
transport, freight, light commercial vehicle	Eco	1.62E-05 t*km	EcoInvent v3.4
transport, freight, lorry, unspecified	Eco	0.00051 t*km	EcoInvent v3.4
Output	Flow type	Quantity	Data source
Ultrapure hydrogen	Eco	1 Nm <sup>3</sup>	SAES / Proton product spec sheets

*On-site generation: PEM on-site generator + adsorber/getter.* The proton exchange membrane (PEM) generator commercialized by Proton delivers 30 Nm<sup>3</sup>/hr, consuming 5.8 kWh / Nm<sup>3</sup> on average. (For consistency check, we compare with Mehmeti et al.<sup>88</sup> who separately report a consumption of 54.6 kWh/kgH<sub>2</sub> = 4.5 kWh/Nm<sup>3</sup>. Balahi et al.<sup>90</sup> report a consumption of 4.775 kWh/Nm<sup>3</sup>). The Proton PEM generator also requires 26.9 L/h of deionized water per hour and 167 L/min coolant. The purifier (adsorber + getter) commercialized by SAES Gas handles a flow of 100 Nm<sup>3</sup>/h at an average power consumption of 26kW, therefore 0.26kWh/Nm<sup>3</sup>. It also consumes 60 L/min of cooling water, therefore 0.036 m<sup>3</sup> water/Nm<sup>3</sup>. Data for the combined processes is presented in Table A.2-11.

Table A.2-11. Process inputs and outputs for onsite generation and purification of hydrogen

Input	Flow type	Quantity	Data source
Electricity	Eco	6.022 kWh	SAES / Proton product spec sheets
DI water	Eco	0.897 kg	Proton product spec sheet
Cooling water	Eco	0.34 m <sup>3</sup>	SAES product spec sheet
Output	Flow type	Quantity	Data source
Ultrapure hydrogen	Eco	1 Nm <sup>3</sup>	SAES / Proton product spec sheets

#### A.2.2.11.2. *Ultrapure nitrogen*

We consider the use of commercially available liquid nitrogen, which is produced via cryogenic air separation and delivered to consumers in the European market as per EcoInvent v3.4.<sup>86</sup> Although the nitrogen produced via this method is of high purity (99.9999%), we consider additional purification on-site using data for a commercially available SAES purifier.

Table A.2-12. Process inputs and outputs for purification of nitrogen for MOVPE application

Input	Flow type	Quantity	Data source
Nitrogen	Eco	1.25 kg	EcoInvent v3.4
Electricity	Eco	3.3E-4 kWh	SAES product spec sheet
Cooling water	Eco	6.4E-4 m <sup>3</sup>	
Output	Flow type	Quantity	Data source
Ultrapure nitrogen	Eco	1 Nm <sup>3</sup>	SAES product spec sheets

#### A.2.2.11.3. *Hydride gases*

Hydride gases arsine and phosphine were taken directly from the EcoInvent v3.4 database.<sup>86</sup> It is known that further purification may be required to reduce acids and humidity that result from cylinder use, and this can be achieved by commercially available purifiers that use an adsorbent medium. However, no specific data for this purification process was available at the time of this report. It is flagged, however, as an important follow-up area due to the potential generation of significant amounts of hazardous waste in the form of adsorbent media.

#### A.2.2.12. *Metalorganic precursors*

We used the input/output data for the synthesis of metalorganic precursors for III-V MOVPE reported by Smith et al. (2018)<sup>91</sup>.

#### A.2.2.13. *Scrubbing of MOVPE and ion implant exhaust gas*

We assumed dry scrubbing systems, in which the main component is an adsorbent granulate. Energy is only required to operate the equipment systems and monitors, but not for the reaction, therefore it was assumed negligible. Based on tests run at Fraunhofer ISE facilities, 17 kg of hydride gases (arsine or phosphine) from an MOVPE reactor were absorbed in 130 kg of granulate.

Granulate composition is not disclosed by manufacturers, but a review of literature, patents, safety data sheets and technical brochures indicates that the industry is moving towards chemisorption by copper oxide catalyst impregnated on a supporting medium of alumina ( $\text{Al}_2\text{O}_3$ ) or silicate ( $\text{SiO}_2$ )<sup>92–95</sup>. Another option is the use of zeolite (a microporous aluminosilicate mineral) exchanged with a copper cation. After adsorption, the granulate

is collected and reprocessed externally into new copper for other industrial uses. No information could be found on intermediate processing steps.

For the zeolite based adsorbent, we modelled the process described Wang and colleagues<sup>96</sup> for the adsorption of arsine, which is similar to the process described by Li and colleagues<sup>97</sup> for phosphine. We chose the best performing alternative presented by the authors, a copper-loaded zeolite, which is produced by impregnating the zeolite in a 50 mL solution of copper II nitrate with a concentration of 0.2 mol/L Cu(NO<sub>3</sub>)<sub>2</sub>. Based on the preparation procedure reported by the authors, the inputs and outputs are:

*Table A.2-13. Process inputs and outputs for purification of scrubbing of arsine and phosphine*

Input	Flow type	Quantity	Data source
Zeolite adsorbent	Eco	7.65 kg	Fraunhofer, personal communication
Hazardous waste, for underground deposit	Eco	-8.65 kg	Calculated as mass of adsorbent + mass of treated gas.
Output	Flow type	Quantity	Data source
III-V waste gas treatment	Eco	-1 kg	Fraunhofer, personal communication

*Table A.2-14. Process inputs and outputs for production of copper zeolite adsorbent granulate*

Input	Flow type	Quantity	Data source
Zeolite powder	Eco	10 g	Wang et al. <sup>96</sup>
Copper II nitrate	Eco	2.95 g	Wang et al. <sup>96</sup> . Based on molar mass of Cu(NO <sub>3</sub> ) <sub>2</sub> . Authors report 10% Cu(II) content by weight in final adsorbent. Starting mass of zeolite is 10 g
Output	Flow type	Quantity	Data source
Zeolite adsorbent	Eco	12.95 g	Wang et al. <sup>96</sup> .

#### A.2.2.14. III-V MOVPE growth on GaAs substrate

*Table A.2-15. Process inputs and outputs for MOVPE III-V growth on GaAs substrate*

Input	Flow type	Quantity	Data source
TMGa	Eco	5.26 g	Aixtron, personal communication
TMIn	Eco	1.23 g	Aixtron, personal communication
TMAI	Eco	3.17 g	Aixtron, personal communication
AsH <sub>3</sub>	Eco	19.96 g	Aixtron, personal communication
PH <sub>3</sub>	Eco	4.15 g	Aixtron, personal communication
H <sub>2</sub>	Eco	0.93 m <sup>3</sup>	Aixtron, personal communication
N <sub>2</sub>	Eco	2.24 m <sup>3</sup>	Aixtron, personal communication
Cooling water	Eco	17.89 m <sup>3</sup>	Aixtron, personal communication
Electricity	Eco	68.33 kWh	Aixtron, personal communication
Hazardous waste treatment	Eco	0.024 kg	Calculated

Output	Flow type	Quantity	Data source
III-V layer area	Eco	2905 cm <sup>2</sup>	Aixtron, personal communication

#### A.2.2.15. Bonding

The bonding process as described by Heitmann et al.<sup>98</sup> requires 4 steps: HF clean, spray pyrolysis, adhesion and hot press. For the hot-press we used parameters from a commercial wafer bonding tool (<https://www.suss.com/en/products-solutions/wafer-bonder/sb6-sb8-gen2>). The tool has a power rating of 4.2kW and can process up to 8 wafers simultaneously. We assumed a bonding time of 20 minutes.

Table A.2-16. Process inputs and outputs for bonding

Input	Flow type	Quantity	Data source
HF	Eco	3.44 g	Fraunhofer ISE, personal communication
Spray pyrolysis solution	Eco	120 mL	Fraunhofer ISE, personal communication
Electricity	Eco	0.175 kWh	Fraunhofer ISE, personal communication
Output	Flow type	Quantity	Data source
Bonding of 1 III-V/Si cell	Eco	1 unit	

Table A.2-17. Process inputs and outputs for bonding of spray pyrolysis solution.

Input	Flow type	Quantity	Data source
Zinc 2,4 pentanedione	Eco	1.7 g	Fraunhofer ISE, personal communication
Methanol	Eco	20.0 g	Fraunhofer ISE, personal communication
Indium trichloride	Eco	1.32 g	Fraunhofer ISE, personal communication
Output	Flow type	Quantity	Data source
Spray pyrolysis solution	Eco	1 L	

There are several routes for the industrial synthesis of zinc 2,4 pentanedione (which is a metal acetylacetone)<sup>99</sup>; we consider a reaction of the zinc chloride salt with acetylacetone and use stoichiometric calculations to estimate the amounts and assume 10% losses.

Table A.2-18. Process inputs and outputs for preparation of zinc 2,4 pentadionate.

Input	Flow type	Quantity	Data source
Vinyl acetate	Eco	0.22 kg	
Zinc chloride	Eco	0.15 kg	

Output	Flow type	Quantity	Data source
Zinc 2,4 pentanedione	Eco	0.34 kg	

Table A.2-19. Process inputs and outputs for synthesis of zinc chloride.

Input	Flow type	Quantity	Data source
Hydrochloric acid	Eco	0.08	
Zinc	Eco	0.07	
Output	Flow type	Quantity	Data source
Zinc chloride	Eco	0.14	

#### A.2.2.16. Lift-off

##### A.2.2.16.1. Laser lift-off

For lift-off practiced on a 10x10mm sample, the total energy consumption of the laser equipment was measured at 0.002 kWh (we disregard power consumption during startup and shutdown, assuming a large number of cells can be processed continuously). To this, we add 0.04 kWh for the ventilation equipment, which must operate after processing on the GaAs sample for safety reasons. The laser stage has an area of 762 x 432 mm, so we assume that 70 x 40 samples can be ventilated at a given time. Extrapolating this linearly to a cell (area 78.3 cm<sup>2</sup>), we get a total of:

$$\left( \frac{0.002 \text{ kWh}}{10 \times 10 \text{ mm}^2} + \frac{0.04 \text{ kWh}}{70 \times 40 \times 10 \times 10 \text{ mm}^2} \right) \cdot \frac{100 \text{ mm}^2}{\text{cm}^2} \cdot \frac{78.3 \text{ cm}^2}{\text{cell}} = \frac{0.16 \text{ kWh}}{\text{cell}} \quad (\text{Eq. A.2-11})$$

##### A.2.2.16.2. Chemical lift-off

To compare the laser lift-off with a chemical method, we modelled a wet chemical process used to etch the bonding layer. Based on projections for state of the arte wet-chemical etching system, we assumed a consumption of 1,25 ml of 50% HF etching solution per wafer. The recyclability of the etching solution is very high, therefore we disregarded the wastewater treatment from this process.

#### A.2.2.17. GaAs substrate reuse and reclaim

We assumed that the GaAs substrate can be reused 100 times. However, this requires periodical chemical-mechanical polishing (CMP) of the GaAs substrate<sup>100</sup> which is done every 5 reuse cycles. We assume 98% process losses.

Table A.2-20. Process inputs and outputs for reclaiming of GaAs substrate

Input	Flow type	Quantity	Data source
CMP slurry	Eco	0.2 L	Matovu et al. <sup>100</sup>
electricity	Eco	2 kWh	

Output	Flow type	Quantity	Data source
Reclaim of 1 GaAs substrate	Eco	1 unit	

Table A.2-21. Energy and material inputs and outputs for CMP slurry

Input	Flow type	Quantity	Data source
Activated silica	Eco	100 g	Matovu et al. <sup>100</sup>
Hydrogen peroxide	Eco	33.33 g	Matovu et al. <sup>100</sup>
Water, deionised		866.67 g	Matovu et al. <sup>100</sup>
Output	Flow type	Quantity	Data source
CMP slurry	Eco	1 L	

#### A.2.2.18. III-V/Si PV electricity generation

The III-V/Si cells can be a drop-in replacement for commercially available single-Si PV systems. To make all infrastructure and BOS components equal in the III-V/Si and single-Si systems, we duplicated the ecoinvent (v3.4) process for generation of 1 kWh from a roof-mounted installation. We then replaced the single-Si cell for the III-V cell in the panel which was supplied to the installation, using the same cell area. The area of cell required to generate a given amount of electricity is inversely proportional to the conversion efficiency of the cell, so we applied the increased efficiency factor to the electricity output of the III-V/Si plant. The efficiency of the single-Si module in ecoinvent is 15.4%, and for the III-V/Si module is 30%, giving a conversion factor of  $(0.3/0.154) = 2.22$ . We applied this directly to the output of the III-V/Si installation, where instead of generating 1kWh it would generate 2.22 kWh with the same ancillary infrastructure and BOS components.

### A.2.3. Sensitivity analysis of technological improvements

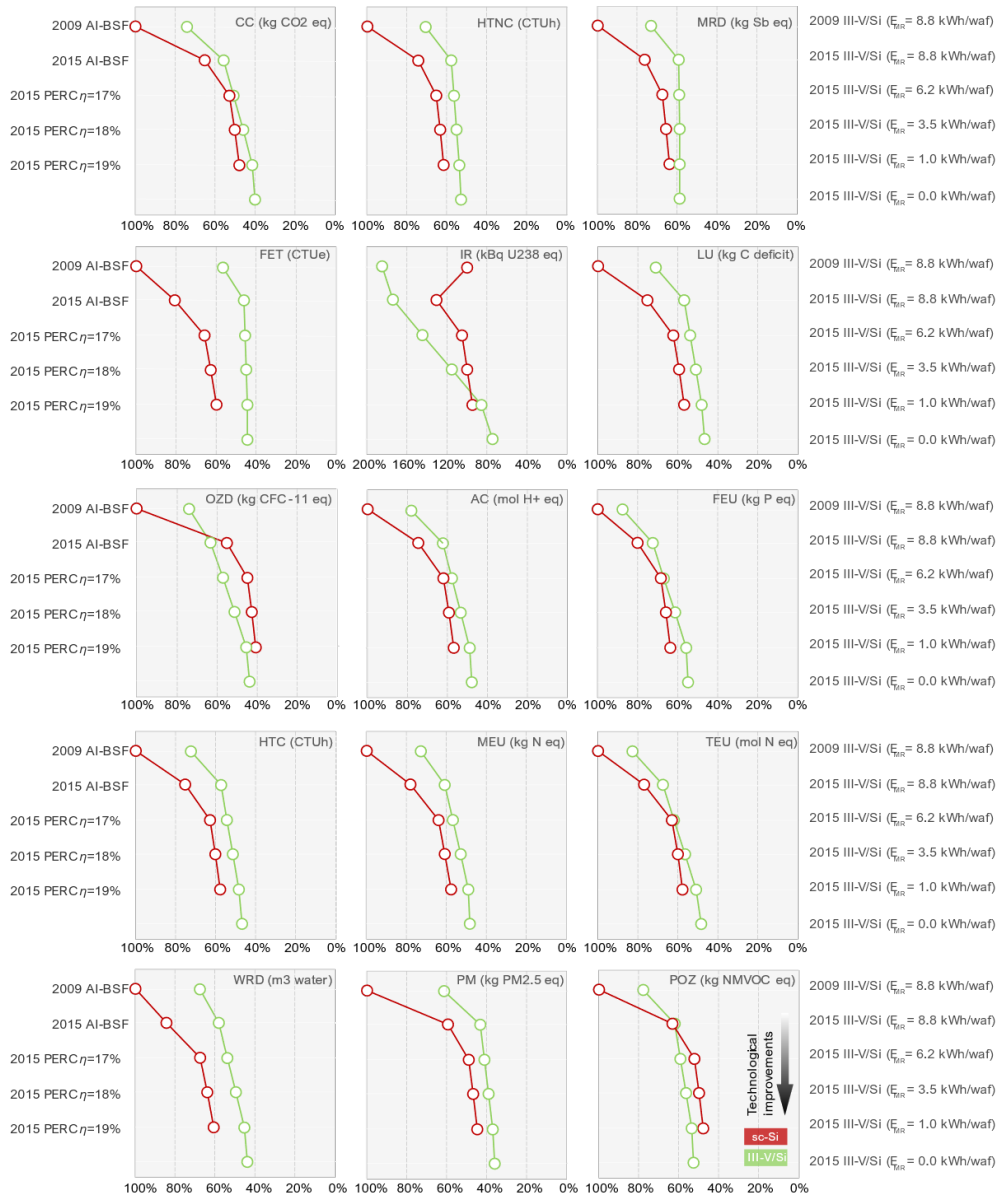


Figure A.2-2 Change in impact scores as a result of technological improvements. 2009: Reference data (2009) for silicon, module and BOS supply chains from ecoinvent v3.4; 2015: Updated IEA PVPS data (2015) for silicon, module and BOS supply chains;  $\eta$ : module efficiency; EMR.: Energy consumption for a single MOVPE run of 37 wafers (2905 cm<sup>2</sup>).

## A.3. Supplementary information to Chapter 4

### A.3.1. Implementation notes: Setting up an uncertain product system

The Bernoulli and Categorical distributions are not available in the most commonly used LCA software packages. They can be implemented in MatLab (or Python, following similar algorithms) using the Binomial and Multinomial distributions, which are a general case of each. Section A.3.1.3 presents an alternative for implementation in publicly available software packages (e.g. OpenLCA, SimaPro, GaBi) that allow the use of uncertain user-defined parameters and formulas.

In the following code snippets, values in blue are examples, which can be replaced by the user according to their case. The code is designed for matrix-based LCA calculations as described by Heijungs and Suh<sup>101</sup>.

#### A.3.1.1. Product system with two alternative, mutually exclusive processes: using the binomial distribution in MatLab.

n = 1;	Number of trials, always 1
x = 4088;	Column number for process X in the technology matrix
y = 4089;	Column number for process Y in the technology matrix
z = 4090;	Column number for process Z in the technology matrix
fx = 2;	Quantity of product from process X going to process Z
Quantity of product from process Y going to process Z	
Px = 0.3;	Probability of process X
T = binornd(n,Px);	Random number from Binomial Distribution. Will give T a value of 1 depending on the probability Px.
A(x,z) = fx·T;	Multiply the flows in the technology matrix by the corresponding trigger value
A(y,z) = fy·(1-T);	

The corresponding function in Python to generate a random number from a binomial distribution, using the same variable designations as above is:

```
numpy.random.binomial(n, Px, size=None)
```

*A.3.1.2. Setting up a product system with three or more alternative, mutually exclusive processes: using the multinomial distribution in MatLab.*

n = 1;	Number of trials, always 1
x = 4088; y = 4089; w = 4090; z = 4091;	Column number for process X in the technology matrix Column number for process Y in the technology matrix Column number for process W in the technology matrix Column number for process Z in the technology matrix
fx = 2; fy = 4; fw = 3;	Quantity of product from process X going to process Z Quantity of product from process Y going to process Z Quantity of product from process W going to process Z
Px = 0.2; Py = 0.2; Pw = 0.6;	Probability of process X Probability of process Y Probability of process W
p = [Px Py Pw];	Create vector with probabilities of each event
T = mnrnd(n,p);	Random number from Multinomial Distribution. Will create a random vector $r$ equal to either [1 0 0], [0 1 0] or [0 0 1] based on the respective probabilities Px, Py and Pz.
A(x,z) = fx·T(1); A(y,z) = fy·T(2); A(w,z) = fw·T(3);	Multiply the flows in the technology matrix by the corresponding trigger value

The corresponding function in Python to generate a random number from a multinomial distribution, using the same variable designations as above is:

```
numpy.random.multinomial(n, p, size=None)
```

*A.3.1.3. Setting up a product system with two or more alternative, mutually exclusive processes. Using the round() function and user-defined (local) parameters in OpenLCA, SimaPro or GaBi.*

OpenLCA and SimaPro allow flow quantities to be entered as formulas rather than fixed numbers. These formulas contain parameters that can be uncertain, hence sampled randomly according to given probability distributions. For the case presented in section A.3.1.1 we can model this as:

$$T = \text{round}(\text{rand}()) + (0.5 - Px) \quad (\text{Eq. A.3-1})$$

Alternatively, we can define a local parameter Pd which has a uniform distribution with min:  $0.5-Px$  and max:  $1+0.5-Px$ . Then,

$$T = \text{round}(Pd) \quad (\text{Eq. A.3-2})$$

Then we can multiply the incoming flows from processes X and Y by the corresponding quantities,  $T$  and  $T-1$ . Note that in the equation above, `rand()` selects a uniformly distributed

value between 0 and 1, which will round to 0 on 50% of the cases and to 1 on the other 50%. By adding  $0.5 - Px$ , the random number will round to 0 on  $Px$  of the cases and to 1 on  $1-Px$  of the cases.

The parameter(s) will be recalculated in each Monte Carlo run, making T adopt a value of 1 or 0 according to the probability  $Px$ .

If there are more than two competing unit processes for the same element of the technology's product system, the same method can be applied by nesting the alternatives so that their combined probabilities result in the desired individual probabilities (see Figure A.3-1). For example, we may have three alternative competing processes X, Y and W with probabilities of 25, 35 and 40% respectively. In this case we set the probability of process XY as 60% ( $25 + 35$ ), the probability of process X as 41.6% (so that when multiplied by 60% we get 25%) and the probability of process Y as 58.3% (so that when multiplied by 60% we get 35%). The probability of process W is set at 40%.

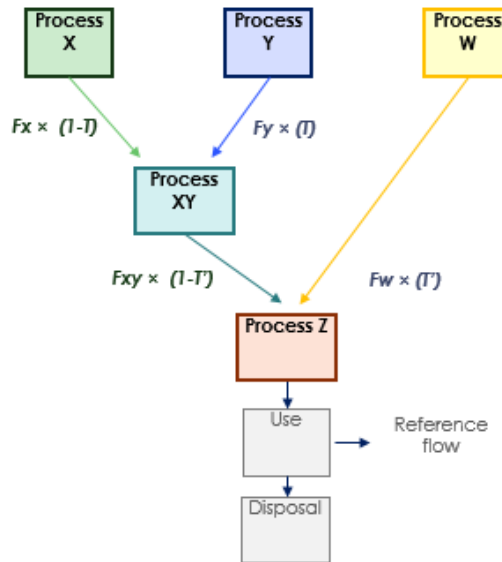


Figure A.3-1 Product system configuration for more than 2 competing alternative unit processes

### A.3.2. Global sensitivity analysis: MatLab implementation

To estimate the Borgonovo delta uncertainty importance measures <sup>102</sup> we used a MatLab function *betaKS3.mat* <sup>103</sup> developed by Elmar Plischke and provided by the authors upon request. The *betaKS3* function takes two main inputs: a matrix *X* with all of the uncertain input parameters (rows) and their sampled value in each MC run (columns), and a vector *Y* with the impact score in each MC run. For all other options we used the default settings.

For the case study we only supplied the uncertain inputs in the foreground system, which were the focus of our investigation. Additional options for the betaKS3 function include the partition size, which we set at 15, and used Monte Carlo sample size of 10,000.

However, the uncertain inputs can also include variable and uncertain parameters from the ecoinvent background. These may be found in both the technology (A) and the environmental (B) matrix. The delta method accounts for interactions between parameters, and only those parameters that somehow affect the output can be provided to the function to reduce computational intensity. Therefore, three filters can be applied to the total set of uncertain input parameters from the A and B matrices to significantly reduce computational time:

- From the A and B matrices, include only uncertain flows from processes that are part of the calculated product system.
- From the B matrix, include only uncertain environmental flows that have a characterization factor for the impact type that is being assessed.
- From the A matrix, include only economic flows from processes that have an environmental flow *at any point upstream* that has a characterization factor for the impact type that is being assessed.

For our case study, we also include the values in each MC run of the different probabilities [Px, Py, Pw...] used to set the triggers for the alternative processes of the emerging technology. These can be appended to the input matrix at the end.

The function returns a vector with the sensitivity index for each parameter in the same order as they were listed in the input matrix  $X$ . The scores can be ranked (while recording the original position) in order to find out the relative importance of each to the variance in the impact score.

Code snippets for implementation of the filters in MatLab are provided below. For the code, we have stored all the uncertain flows in the LCA database along with their position (row | column) and their MC sampled values in two matrices: *inDA* (economic flows), *inDB* (environmental flows). These matrices have the following structure:

Row	Col	Run 1	Run 2	Run 3...	...Run N
1	1	3.26	3.17	3.48	3.21
1	2	0.24	0.23	0.25	0.24
1	5	1.17	1.22	1.09	1.21
...	...	...	...	...	...
# flows	# processes	25.38	24.17	27.19	23.02

In the code below, we apply the two filters (i) and (ii) to these matrices, copying them subsequently to *inDA* → *inDAf1*, and *inDB* → *inDBf1* → *inDBf2*.

*Apply filter (i) to matrices A and B:*

N = 10000	Number of Monte Carlo runs
s = A\f;	Calculates the scaling vector for the demand vector f, from the technology matrix A.
inDAf1 = [inDA zeros(size(inDA,1),1)]; inDBf1 = [inDB zeros(size(inDB,1),1)];	Add a column of zeros at the end of each matrix to place tag
for i = 1:size(inDAf1,1) if s(inDAf1(i,2))==0 inDAf1(i,N+3)=1; end end	If process is not part of product system, scaling vector in that row==0. Tag that row with a 1.
for i = 1: size(inDBf1,1) if s(inDBf1(i,2))==0 inDBf1(i,N+3)=1; end end	Repeat as above, this time for B matrix.
inDAf1(inDAf1(:,size(inDAf1,2))==1,:)=[]; inDBf1(inDBf1(:,size(inDBf1,2))==1,:)=[];	Delete rows with unused processes that are tagged with 1.

Apply filter (ii) to matrix B:

Iref = 482  envflowsCC = find(Q_mat(Iref,:));  inDBf2 = inDBf1(ismember(inDBf1(:,1), envflowsCC), :);	Row position for impact type in Q matrix.  Find the flows in the Q matrix that have a characterization factor for impact <i>Iref</i> . The function <i>find()</i> returns the index (column) for non-zero values in row <i>Iref</i> of the Q matrix.  Copy to inDBf2 only those flows that have been listed in envflowsCC.
---	--

Prepare input matrix for GSA and run GSA:

We can now concatenate the inputs from A and B matrices along with the uncertain foreground parameters and triggers. We have previously stored the randomly sampled foreground input parameters in matrix *inPar* with each row representing each parameter (including the triggers) and each column the corresponding value for each MC run. We have also stored the impact assessment results for the impact category in a vector *Ygsa*, with one result for each run.

Xgsa = cat(1,inDAf1,inDBf2);  Xgsa(:,[1 2]) = [];  Xgsa(:,end) = [];	Concatenate the A and B inputs into a single matrix  Delete first two columns with position information  Delete last column with the tag from filter (i)
--	--

Xgsa = cat(1, Xgsa, inPar);	Concatenate the A and B inputs with the foreground uncertain input parameters and triggers
Xgsa = transpose(Xgsa);	Transpose the matrix
d = deltamim(Xgsa, Ygsa);	Run <i>deltamim</i> function. <i>d</i> will contain a vector with the sensitivity indices.

Note: All uncertain inputs in the background and foreground are pre-sampled and stored in arrays, prior to running the Monte Carlo simulation, in order to ensure that the sampling of compared systems is dependent as recommended by Henriksson et al.<sup>104</sup> In each run, the Monte Carlo simulation picks the same pre-stored value for both systems.

### A.3.3. Case study: process descriptions and input/output data

#### A.3.3.1. Fingers: seed layer (nano) inkjet printing

Materials: The pattern to be printed on the cell for the seed layer consists of 6 fingers 2 mm wide, 75 mm long and 0.1 µm thick on average. The total quantity of nanoink required is calculated by the total volume of this pattern multiplied by the density of each nanoink (reported by the manufacturers). To this quantity, we add 10% to account for ink that remains in the filter and is discarded as hazardous waste. Therefore, for each type of ink we have the following inputs, per cell:

$$\begin{array}{lllll} \# \text{fingers} & \text{Finger width} & \text{Finger length} & \text{Finger thickness} & \text{Ink density Loss factor} \\ & & & & \text{(Eq. A.3-3)} \\ 6 \cdot \left(2 \text{ mm} \cdot \frac{1 \text{ m}}{1E3 \text{ mm}}\right) \cdot \left(75 \text{ mm} \cdot \frac{1 \text{ m}}{1E3 \text{ mm}}\right) \cdot \left(0.1 \mu\text{m} \cdot \frac{1 \text{ m}}{1E6 \mu\text{m}}\right) \cdot \frac{1.27E3 \text{ kg}}{\text{m}^3} \cdot 110\% & = 1.25E-7 \text{ kg Cu ink} \\ 6 \cdot \left(2 \text{ mm} \cdot \frac{1 \text{ m}}{1E3 \text{ mm}}\right) \cdot \left(75 \text{ mm} \cdot \frac{1 \text{ m}}{1E3 \text{ mm}}\right) \cdot \left(0.1 \mu\text{m} \cdot \frac{1 \text{ m}}{1E6 \mu\text{m}}\right) \cdot \frac{1.45E3 \text{ kg}}{\text{m}^3} \cdot 110\% & = 1.44E-7 \text{ kg Ag ink} \end{array}$$

Printer electricity. The current sample being tested is approx. 10 cm. long and takes 5 minutes to print, with only 2 nozzles in use out of a total possible of 210. We estimate the printing speed as:

$$\frac{10 \text{ cm}}{5 \text{ min}} \cdot \frac{210 \text{ nozzles}}{2 \text{ nozzles}} \cdot \frac{60 \text{ min}}{1 \text{ h}} \cdot \frac{1 \text{ m}}{100 \text{ cm}} = \frac{126 \text{ m}}{\text{h}} \quad \text{(Eq. A.3-4)}$$

From the data above, the total length of the 6 printed fingers is 0.45 m, and the printer has a maximum power rating of 1kW. We assume it operates at 75% power on average. To calculate electricity consumption of the printing process (per cell) we have:

$$\frac{0.45 \text{ m}}{\text{cell}} \cdot \frac{1 \text{ h}}{126 \text{ m}} \cdot 1 \text{ kW} \cdot 75\% = \frac{0.027 \text{ kWh}}{\text{cell}} \quad \text{(Eq. A.3-5)}$$

### A.3.3.2. Fingers: seed layer sintering

Laser electricity: The length of the pattern that must be sintered is calculated from the data in the previous section (0.45 m). We use a laser scan speed of 0.01 m/s, and the optical power delivered by the laser is 1.4 W. The wall-plug to optical efficiency of YAG type lasers is typically around 25% <sup>84</sup>, so we estimate the electricity consumption for laser sintering as:

$$\frac{0.45 \text{ m}}{\text{cell}} \cdot \frac{\text{s}}{0.01 \text{ m}} \cdot \frac{1 \text{ h}}{3600 \text{ s}} \cdot 1.4E - 3 \text{ kW} \cdot \frac{1}{25\%} = \frac{5.6E - 5 \text{ kWh}}{\text{cell}} \quad (\text{Eq. A.3-6})$$

Materials: Laser-sintering of both Cu and Ag ink is done in open air.

### A.3.3.3. Fingers: electroplating

Electroplating consists of submerging the cell with the seed pattern in an electrolyte bath, where the patterned cell will serve as an ion-receiving cathode and a copper anode in the solution will serve as a cathode. The electrolyte solution consists of a mix of cupric sulfate and sulfuric acid. Driving an electric current through the solution will force the metallic ions from the cathode to deposit on the seed pattern until the desired geometry is obtained.

Electricity: A conventional electroplating setup is used, where 10 mA of applied current with an average voltage of 0.5 V provides 250 nm of plating per minute. The electrical power can be calculated from the current and voltage:

$$P = I \cdot V = \left(10 \text{ mA} \cdot \frac{1 \text{ A}}{1000 \text{ mA}}\right) \cdot (0.5 \text{ V}) = 5E - 3 \text{ W} = 5E - 6 \text{ kW} \quad (\text{Eq. A.3-7})$$

The amount of electricity consumed is calculated by multiplying the power by the time required to plate the desired finger thickness of 12.5 μm.

$$\frac{5E - 6 \text{ kW}}{\text{cells}} \cdot \frac{1 \text{ min}}{0.25 \mu\text{m}} \cdot 12.5 \mu\text{m} \cdot \frac{1 \text{ h}}{60 \text{ min}} = \frac{4.16E - 6 \text{ kWh}}{\text{cell}} \quad (\text{Eq. A.3-8})$$

Materials: Pure metal anodes donate the ions that ultimately deposit on the pattern (cathode). The ions are first passed from the electrolyte solution to the cathode and are then replenished from the anode to the solution. Therefore, the anode is sacrificed according to the amount of metal deposited in the cell, and we assume 10% losses.

$$(\text{Eq. A.3-9})$$

$$\text{cu: } 6 \cdot \left(2 \text{ mm} \cdot \frac{1 \text{ m}}{1E3 \text{ mm}}\right) \cdot \left(75 \text{ mm} \cdot \frac{1 \text{ m}}{1E3 \text{ mm}}\right) \cdot \left(12.4 \mu\text{m} \cdot \frac{1 \text{ m}}{1E6 \mu\text{m}}\right) \cdot \frac{8.96E3 \text{ kg}}{\text{m}^3} \cdot 110\% = 1.09E - 4 \text{ kg C}$$

We consider a standard cupric sulfate electrolyte solution that consists of 200 g cupric sulfate and 25 mL sulfuric acid in sufficient deionized water to prepare 1 L of electrolyte solution. This amount of solution is used for electroplating on one cell; however, we consider that it can be used for the production of 10-100 wafers based on lab experience, and test the sensitivity of this parameter.

### A.3.3.4. Busbars: screen printing

Screen printing electricity: We use data from a screen printer running a squeegee motor with a power of 1.16 kW. The printer can process a sheet of 400x400mm in 30 seconds.

$$\frac{1 \text{ sheet}}{4 \text{ cells}} \cdot 1.16 \text{ kW} \cdot 30 \text{ s} \cdot \frac{1 \text{ h}}{3600 \text{ s}} = \frac{2.41E - 3 \text{ kWh}}{\text{cell}} \quad (\text{Eq. A.3-10})$$

Curating electricity: Cu busbars are grown over the Ag or Cu fingers by screen-printing. However, instead of co-firing, the Cu busbars are curated at lower temperature (250°C) in an atmosphere of pure nitrogen<sup>85</sup>. This is done in a furnace that has a power rating of 3.4 kW and can process 1000 cells per batch, for a curating time of 10 minutes.

$$\frac{3.4 \text{ kW}}{1000 \text{ cells}} \cdot 10 \text{ min} \cdot \frac{1 \text{ h}}{60 \text{ min}} = \frac{5.67E - 4 \text{ kWh}}{\text{cell}} \quad (\text{Eq. A.3-11})$$

Materials: We consider 3 busbars, 1 mm wide, 156 mm long and 13.5 μm thick on average. We assume 10% losses from the paste during screen-printing. Per cell, we have:

$$(\text{Eq. A.3-12})$$

$$3 \cdot \left(1 \text{ mm} \cdot \frac{1 \text{ m}}{1E3 \text{ mm}}\right) \cdot \left(156 \text{ mm} \cdot \frac{1 \text{ m}}{1E3 \text{ mm}}\right) \cdot \left(13.5 \mu\text{m} \cdot \frac{1 \text{ m}}{1E6 \mu\text{m}}\right) \cdot \frac{8.96E3 \text{ kg}}{\text{m}^3} \cdot 110\% = 6.23E - 5 \text{ kg Cu}$$

## A.4. Supplementary information to Chapter 5

### A.4.1. Model overview

This risk assessment was conducted in six integrated steps:

- III-V/Si PV electricity demand scenarios: Projected the expected PV demand (in MW<sub>p</sub> or GW<sub>p</sub>) in each geographical scale over a period of 100 years using logistic growth curves.
- Dynamic stock flows: Determined the quantity of III-V/Si PV panels (in m<sup>2</sup> of PV installation) manufactured, installed, and recycled/incinerated/landfilled in each year to meet the electricity demands of the previous step.
- Emissions: Determined the quantities of III-V materials emitted to the environment from III-V/Si PV panels at each life cycle stage.
  - *Manufacturing*: Emissions from this phase were deemed negligible as all waste goes to underground hazardous waste storage and/or is reused.
  - *Use phase*: Calculated the emissions that may occur from panel breakage which exposes the III-V materials in the PV cells to leaching during rain events.
  - *End-of-life phase*:
    - ☒ Recycling: no direct emissions to the environment were considered during PV materials separation and repurposing, only the generation of waste.
    - ☒ Incineration: Calculates emissions of III-V materials that vaporize and are not captured by the abatement system, escaping to air.
    - ☒ Landfilling: Calculates emissions from III-V materials that leach from the waste to the landfill leachate, and later escape the landfill through uncontrolled leakage to the surrounding soil. Also calculates emissions that can volatize to air in the landfill.
- Environmental fate: Models the distribution of emitted III-V materials (in kg) in each environmental compartment in each scale and calculates the predicted environmental concentrations (PEC).
- Risk Quotient: Evaluates the risk as a ratio of predicted environmental concentrations (PEC) to concentrations at which no observable effects are reported (PNEC).

These steps are described in detail in the following sections, along with the assumptions and calculation notes. The values and probability distributions taken for all model input parameters are listed in Table A.4-2.

## A.4.2. Demand scenarios

Demand scenarios for three geographical scales were modelled; one for Europe (continental, “SKY\_EUR”), one for the city of Amsterdam (regional, “RES\_AMS”), and an intentionally loaded smaller area ( $\sim 16 \text{ km}^2$ ) containing a floating utility-scale PV plant with surrounding rooftop PV and EOL treatment facilities within it (local, “UTI\_LOC”). The scales are embedded in the model, so that the PV demand (and corresponding emissions) in the local scale is added to the regional scale, and the regional scale is added to the continental scale. In the SimpleBox fate models, materials are allowed to be transported across scales.

With an expected 28% panel conversion efficiency, III-V/Si panels will have a rating of  $280 \text{ W}_p/\text{m}^2$ . This is equivalent to the power output of the panel under standard irradiance conditions of  $1000 \text{ W}/\text{m}^2$ . The rating can also be expressed in terms of efficiency, as the ratio of power output to power input. To translate PV installed capacity to PV installation size (as total Area of panels, in  $\text{m}^2$ ) we used Equation A.4-1.

$$Area = \frac{PV \text{ Capacity}}{Rating} = \frac{PV \text{ Capacity}}{\text{efficiency} \cdot 1000 \text{ W}/\text{m}^2} \quad (\text{Eq. A.4-1})$$

### A.4.2.1. Continental scale: Europe

We modelled a first scenario based on possible future electricity demand in Europe according to the Shell Sky Scenario<sup>105</sup>, which sets the most ambitious targets for electrification and solar generation in Europe from the different scenarios presented by Shell. In this scenario, total PV electricity demand will rise to 18.43 EJ (=5,138 TWh) by the year 2100, split equally between distributed and utility. If the IEA’s “High GaAs” market shares are taken 15% of the utility share and 5% of the rooftop share would be taken by III-V/Si panels, the installed capacity of III-V/Si panels is 10%, or 513.8 TWh. We translate this electricity demand to installed capacity by assuming a 1200 kWh/kW<sub>p</sub> average yield in Europe<sup>106</sup>, although this can vary if the location of new PV installations shifts significantly to the north or south. Based on these data, we used a logistic growth curve (equations A.4-2 and A.4-3) to project installed capacity at any given time  $C(t)$ , starting with an initial capacity addition of  $C_0 = 100 \text{ MW}_p$  in the year 2031 and stabilizing at  $C_f = 430 \text{ GW}_p$ . We took the growth rate  $k = 14.1\%$  from the 75<sup>th</sup> percentile of 1100 different PV deployment scenarios in Europe that were reviewed and harmonized by Jaxa-Rozen et. al.<sup>107</sup>

$$C(t) = \frac{C_f}{1+A \cdot e^{-kt}} \quad (\text{Eq. A.4-2})$$

$$A = \frac{C_f - C_0}{C_0} \quad (\text{Eq. A.4-3})$$

Of the total amount of III-V/Si PV panels produced each year, we assumed 25% would be installed on rooftop installations, while 75% would be installed in utility-scale plants, following the IEA’s “High GaAs” scenario.<sup>108</sup> We further assumed that a fraction of utility-scale corresponding to 13.3% of utility ( $\sim 10\%$  of total generation) is supplied by floating

structures on surface water bodies (lakes) based on projections made by Cazzaniga et al. for floating PV installations.<sup>109</sup> In lieu of data, we assumed an equal split between rooftop installations that drain to freshwater and those that drain to soil (Figure A.4-1).

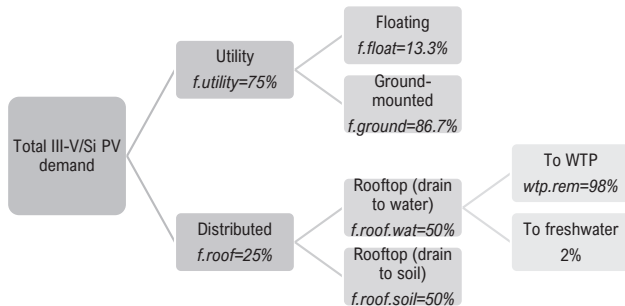


Fig A.4-1. Projected distribution of III-V/Si modules in Europe based on installation type and location.

#### A.4.2.2. Regional scale: Amsterdam area

The second scenario we modelled was based on the stated policies of the Amsterdam municipality<sup>110</sup>. The number of installed solar panels has grown by approximately 50% annually from 2012 to mid-2019. The city's aspiration is to reach 550 MW by 2030, which is half of the total potential of roofs (large and small). Afterwards, the city is committed to "leave no roof unused", with a roof potential of 1100 MW. Floating PV and ground-based installations will be kept as an option only if the targets are not achievable otherwise. Following these stated aspirations, for this scenario we assume III-V/Si enters the market after 2030 with an initial installed capacity of 100 kWp and grows at the pace of 20% annually to take up 10% of the total rooftop potential. As per Equations A.4-2 and A.4-3, this can be represented by setting  $C_0 = 0.1$  MW,  $C_f = 110$  MW, and  $k = 0.2$ . The distributions according to type of installation are shown in Figure A.4-2.

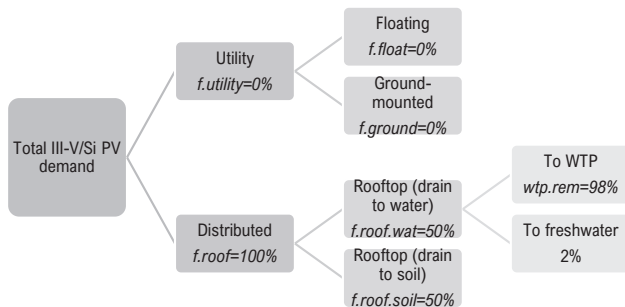
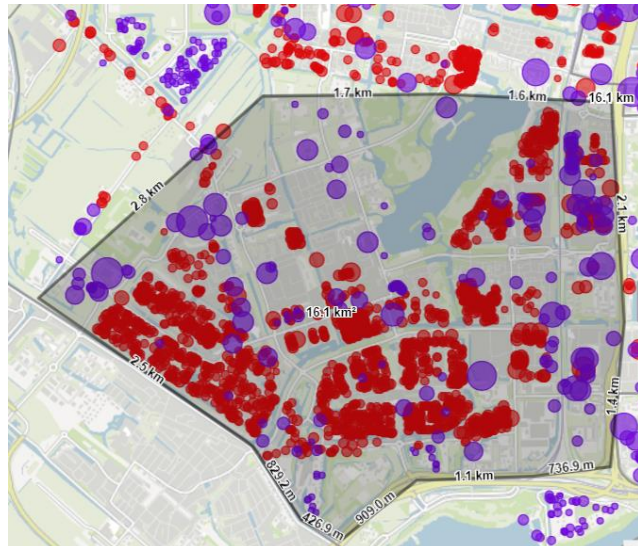


Fig A.4-2. Projected distribution of III-V/Si modules in Amsterdam based on installation type and location.

#### A.4.2.3. Local scale: Floating utility plant and surrounding rooftop installations

The third scenario represents a very localized situation, largely based on the current status (2020) of the Sloterplassen lake area in Amsterdam. The number of rooftop panels currently installed in the encircled area (Figure A.4-3) is approximately 50,000. For this scenario, we

assume all the panels are replaced for III-V/Si panels in 2030. We also assumed all panels in this area will drain directly to soil, or towards the lake. In addition to this, 50 MW of III-V/Si panels are assumed to be installed in 2030 as a floating utility installation on the lake, taking up approximately 20% of the lake area.



*Fig A.4-3. Current PV installations around the Sloterplassen lake in Amsterdam (red: on houses, purple: on non-houses or mixed).\**

#### A.4.3. Stock flows

According to the current European Union regulations, 85% of solar panels by weight must be collected for recycling.<sup>111</sup> The base (conservative) case considers current PV recycling practices, which largely focus on the aluminum framing, glass, and plastic components of the panel while the cell is discarded (Figure A.4-4). Based on interviews we conducted with industry representatives, it is believed that if an amount of arsenic in the order of 100 ton per year would become available for recycling, then this additional recycling step would become economically feasible. This alternative is tested in a sensitivity analysis where  $f.rec.reu=98\%$  and  $f.rec.rej=2\%$ .

---

\*<https://maps.amsterdam.nl/zonnepanelen/?LANG=en>.

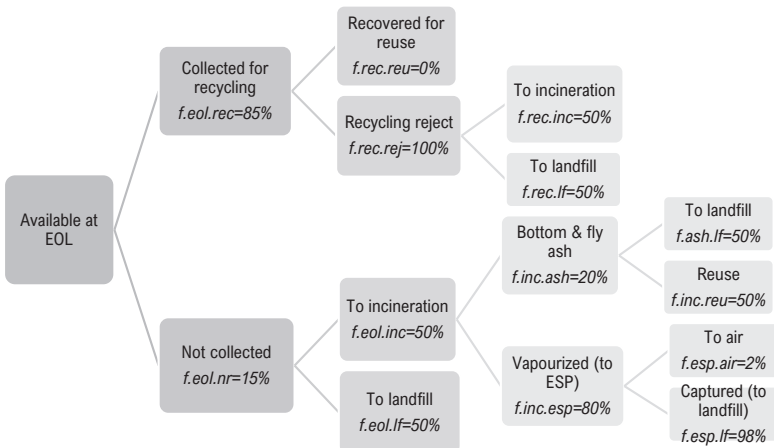


*Fig A.4-4. Distribution of III-V/Si panels at EOL. Percentage values represent the base (conservative) case with no arsenic recovery during recycling.*

## A.4.4. Emissions

### A.4.4.1. Use phase<sup>†</sup>

The model supposes III-V materials emissions during the use phase may occur if there is leaching from broken panels during rain events. The potentially released amounts were determined by calculating the release per second per broken panel, and multiplying this by the exposure time to rainwater, number of panels, and fraction of panels with glass breakage. The release of arsenic/gallium/indium per broken panel is dependent on the speciation in the panel which consists of two factors: dissolution at the crack surface of directly exposed material (modelled according to Celik et al.<sup>67</sup>) and transport of arsenic on non-exposed parts that gets dissolved by water ingress and is transported to the crack where it is then released.

The total release can be expressed as:

$$R.system = (R.crack + trans.crack) \cdot t.exp \cdot n.system \cdot f.cracked \quad (\text{Eq. A.4-4})$$

Where:

*R.system* = total release of a metal from a specific speciation from the PV system in g/year

*R.crack* = dissolution rate of metal where the metal is directly exposed to the solvent due to the crack in g/s

*trans.crack* = transport of dissolved metal from the rest of the panel to the crack in g/s

---

<sup>†</sup> The “use phase” calculations presented in this section are based on the RIVM/Wageningen University and Research internship report by Matthias Hof, “Environmental risk assessment of photovoltaic-panels applied on surface waters” (April 15, 2021). Supervised by Joris Quik, Michiel van Kuppevelt (RIVM), Bart Koelmans (WUR).

*t.exp* = exposure time to solvent (rainwater) per year in s/year

*n.system* = number of panels in the PV system

*f.cracked* = fraction of panels in the system with glass panel breakage

The exposure time to solvent (rainwater) per year is calculated as:

$$t.exp = t.rain \cdot t.remove / 365 \quad (\text{Eq. A.4-5})$$

Where:

*t.rain* = days of rain per year

*t.remove* = days until removal after breakage of panel

The dissolution rate of arsenic directly exposed at the cracks of a broken panel can be calculated as:<sup>67</sup>

$$R.crack = A.crack \cdot \left(\frac{D}{d}\right) \cdot (Cs - Cb) \quad (\text{Eq. A.4-5})$$

Where:

*A.crack* = cumulative surface area of cracks in m<sup>2</sup>

*D* = diffusion coefficient of metal in m<sup>2</sup>/s

*d* = thickness boundary layer of diffusion in m

*Cs* = saturated mass concentration of metal in water in g/m<sup>3</sup>

*Cb* = concentration of metal in bulk solvent (rainwater) in g/m<sup>3</sup>

In Equation A.4-5, the saturated mass concentration *Cs* is given by:

$$Cs = MW \cdot Ss \quad (\text{Eq. A.4-6})$$

Where:

*MW* = Molecular weight of metal atom in g/mol

*Ss* = saturated molar concentration of metal ions in mol/l

The saturated molar concentration *Ss* is:

$$Ss = \left(\frac{x}{y}\right)^{\frac{y}{x+y}} \cdot Ksp^{\frac{1}{x+y}} \quad (\text{Eq. A.4-7})$$

Where:

*x* = number of metal ions in soluble speciation

*y* = number of anions in soluble speciation

*Ksp* = solubility constant of soluble speciation

Finally, the cumulative crack surface is calculated as:

$$A.crack = n.cr \cdot (W.cr \cdot L.cr) \quad (\text{Eq. A.4-8})$$

Where:

*n.cr* = number of cracks

$W_{cr}$  = width of the crack in m

$L_{cr}$  = length of the crack in m

In addition to direct dissolution at the crack surface, III-V materials in the rest of the panel may be exposed to the solvent through the ingress of rainwater. We assumed that ingressed water is continuously present in the panel, and the concentration of dissolved III-V materials in the ingressed water was assumed to be saturated due to the long residence time. The release of metal through the crack can thus be described by the transport from its position in the panel to the crack through diffusion.

The transport of dissolved metal to crack is calculated as:

$$trans.\ crack = J.\ crack \cdot A.\ cr.\ sides \quad (\text{Eq. A.4-9})$$

Where:

$J.\ crack$  = the flux of dissolved metal to the crack in g/m<sup>2</sup>/s

$A.\ cr.\ sides$  = the surface of the diffusion interface between the panel and the crack, which is the surface of the sides of the crack in m<sup>2</sup>.

The flux of dissolved metal to crack is given by:

$$J.\ crack = D \cdot \frac{Cs - Cb}{distance.\ cr} \quad (\text{Eq. A.4-10})$$

Where:

$distance.\ cr$  = the average travel distance of the metal from any point in the panel to the crack

The surface of the diffusion interface can be calculated by the width and length of the crack, and the “depth” of the crack, or the thickness of the space between sheets of the panel through which the rainwater can ingress. Due to the possibility of multiple cracks on the panel, the total surface of the diffusion interface is the sum of the sides of multiple cracks. The total surface of the diffusion interface can be calculated as follows:

$$A.\ cr.\ sides = (n.\ cr \cdot 2(W.\ cr + L.\ cr)) \cdot D.\ cr \quad (\text{Eq. A.4-11})$$

Where:

$D.\ cr$  = depth of crack in m.

If the panel is regarded as a two-dimensional sheet, the average travel distance of dissolved metal from any point in the panel to the crack can be described by the average distance between two random points in a rectangle of a certain size. The average distance between two random points in a rectangle is described by Mathai et al.<sup>112</sup>:

$$\begin{aligned}
\text{avg. dis. panel} &= 1/15 \cdot ((L.\text{panel}^3)/(W.\text{panel}^2)) \\
&\quad + (W.\text{panel}^3)/(L.\text{panel}^2) \\
&\quad + d(-(L.\text{panel}^2)/(W.\text{panel}^2)) \\
&\quad - (W.\text{panel}^2)/(L.\text{panel}^2)) \\
&\quad + 5/2((W.\text{panel}^2)/(A.\text{panel}) \ln ((L.\text{panel} \\
&\quad + LW)/(W.\text{panel})) \\
&\quad + (L.\text{panel}^2)/(W.\text{panel}) \ln ((W.\text{panel} \\
&\quad + LW)/(L.\text{panel})))
\end{aligned} \tag{Eq. A.4-12}$$

Where:

$\text{avg. dis. panel}$  = the average distance between two random points in a rectangle with sides  $L.\text{panel}$  and  $W.\text{panel}$  in m

$L.\text{panel}$  = the length of the panel in m

$W.\text{panel}$  = the width of the panel in m

$$LW = (L.\text{panel}^2 + W.\text{panel}^2)^{1/2}$$

$$L.\text{panel} > W.\text{panel}$$

Because of the possibility of multiple cracks forming on the panel, the actual distance from any point on the panel to the crack would be smaller than the average distance between two points. As far as we are aware, there is no formula for the average distance between multiple random points in a rectangle. To approximate this decrease in distance with multiple cracks, the average distance calculated by Eq. A.4-12 was divided by the number of cracks on the panel:

$$\text{distance. cr} = \frac{\text{avg. dis. panel}}{n.\text{cr}} \tag{Eq. A.4-13}$$

This underestimates the actual distance when cracks are not uniformly distributed, however this was deemed preferable over overestimating the distance as the latter leads to underestimating the release of metals and resulting ecotoxicological risk.

Finally, the amount of metal that can be released through direct dissolution at the crack with the Celik et al.<sup>67</sup> formula was limited to the amount of metal directly exposed to the outside environment (using an IF statement):

$$\text{IF}((R.\text{crack} \cdot t.\text{exp}) < Mu.\text{crack}; (R.\text{crack} \cdot t.\text{exp}); Mu.\text{crack}) \tag{Eq. A.4-14}$$

The mass of metal directly exposed at crack is equal to:

$$Mu.\text{crack} = Mu.\text{spec} \cdot f.\text{crack} \tag{Eq. A.4-15}$$

The amount of metal of specific speciation in panel is:

$$Mu.\text{spec} = Mu.\text{PVarea} \cdot L.\text{panel} \cdot W.\text{panel} \cdot f.\text{spec} \tag{Eq. A.4-16}$$

The fraction of panel surface exposed by crack is:

$$f.\text{crack} = \frac{A.\text{crack}}{A.\text{pv.panel}} \tag{Eq. A.4-17}$$

Where:

$Mu.\text{crack}$  = amount of metal directly exposed to outside environment in g

$Mu.\text{spec}$  = total weight of metal of specific speciation in panel in g

$A.\text{crack}$  = total crack surface area in m<sup>2</sup>

$Mu.PVarea$  = weight of metal per surface area of PV panel in g/m<sup>2</sup>

$f_{\text{spec}}$  = ratio of metal from specific speciation to total amount of that metal in the panel

Similarly, the total amount of metal that can be released from the panel through dissolution in ingressed water and subsequent diffusion can be limited by:

$$IF((trans.\text{crack} \cdot t.\text{exp}) < Mu.\text{ingress}; (trans.\text{crack} \cdot t.\text{exp}); Mu.\text{ingress}) \quad (\text{Eq. A.4-18})$$

The amount of metal of specific speciation in panel that is not directly exposed by crack is:

$$Mu.\text{ingress} = Mu.PVarea \cdot A.\text{pv.panel} - Mu.\text{crack} \quad (\text{Eq. A.4-19})$$

Where:

$Mu.\text{ingress}$  = weight of metal not directly exposed to outside environment in g.

#### A.4.4.2. End-of-life

##### A.4.4.2.1. Landfilling

A simplified landfill model based on EPA's Composite Model for Leachate Migration with Transformation Products (EPACMTP)<sup>113,114</sup> was used to determine how much arsenic will dissolve from the PV discarded in landfills into the landfill leachate, and how much of the leachate containing these elements will escape the landfill into the surrounding environment. For simplicity, we assumed each cohort (yearly installation) will be disposed in a new landfill cell, all of which constitute monofills (only PV waste).

Once a landfill cell has been closed, it is expected that the concentration of an element in the leachate will decrease over time as the available quantity embedded in the waste is depleted. As per the EPACMTP model, this constitutes a "depleting source scenario", where the leachate concentration at a given time ( $t$ ) is a linear function of the remaining concentration in the waste  $C_w(t)$ :

$$C_L(t) = K_w \cdot C_w(t) \quad (\text{Eq. A.4-20})$$

In equation A.4-20,  $K_w$  is a waste/leachate partitioning coefficient.  $K_w$  values for arsenic were suggested by EPA<sup>115</sup>, based largely on previously reported leachate extraction test results and modeling using the MINTEQA2 geochemical speciation model.

A mass balance can then be performed at any given time  $t$ , where the difference between the initial concentration in the waste and the concentration at time  $t$  should equal the total amount lost via leaching. Assuming all the waste is composed of the same PV waste (monofil), this mass balance can be expressed as:

$$A_W \cdot D_{LF} \cdot \rho_W \cdot \frac{dC_L}{dt} = A_W \cdot I \cdot C_L(t) \quad (\text{Eq. A.4-21})$$

$C_W$  can be substituted for  $C_L$  using equation A.4-20 and equation A.4-21 can be rearranged to obtain:

$$\frac{dC_L}{dt} = \frac{-I}{D_{LF} \cdot \rho_W \cdot K_W} C_L \quad (\text{Eq. A.4-22})$$

Equation A.4-22 can be integrated to give:

$$C_L(t) = C_L^0 \cdot \exp \left\{ \left( \frac{-I}{D_{LF} \cdot \rho_W \cdot K_W} \right) t \right\} \quad (\text{Eq. A.4-23})$$

In equation A.4-23,  $C_L^0$  represents the initial concentration of the element in the leachate at the time of landfill cell closure.

A small fraction of arsenic present in the landfill waste was assumed to be volatized due to biological processes. We took a range of values of 0.02-0.1% as reported by Webster et al.<sup>116</sup> for microbially mediated volatilization in anaerobic environments. It is likely that or monofils with reduced microbial activity this value is on the lower range if not negligible. This process is assumed to occur within the simulation time step of 1 year, and so is immediately subtracted from the amount available for leakage.

#### A.4.4.2.2. Incineration

During incineration, arsenic in PV waste can be reduced to bottom ash or volatized. In the latter case, it will join the flue gas which is mostly captured by an electrostatic precipitator (ESP) while a small fraction escapes to air. Arsenic in bottom ash and captured in the ESP (fly ash) are assumed to be sent to the same PV landfill cells used described in section A.4.4.2.1.

We based our assumptions on a study by Uryu et al.<sup>117</sup>, who modelled the distribution of arsenic in GaAs FET semiconductors in mobile phones that are burned in hazardous waste incineration plants in Japan. Of the incinerated amount, 90% of arsenic was present in the gas phase at high incineration temperatures. 0.2% of arsenic present in the gas was found to escape to air while the remaining fraction (bottom ash and fly ash) was sent to a landfill.

### A.4.5. Environmental fate

The Excel spreadsheets and annotated R scripts to run the fate model as described in Section 5.2.5 of Chapter 5 are available at <https://github.com/jormercury/SimpleBox>. The emissions were sent to specific compartments in SimpleBox as indicated in Table A.4-1.

Table A.4-1 Receiving compartments for Use and EOL phase emissions

Emission	SKY_EUR	AMS_RES	UTI_LOC
Use phase – leaching, utility (ground)	Continental agricultural soil, s2C	Regional agricultural soil, s2R	Local soil, sL
Use phase – leaching, utility (floating)	Continental freshwater, w1C	Regional freshwater, w1R	Local water, wL
Use phase – leaching, distributed	Continental freshwater, w1C	Regional freshwater, w1R	Local water, wL
EOL phase – incineration	Continental air, aC	Regional air, aR	Local air, aL
EOL phase – landfill leaching	Continental agricultural soil, s2C	Regional natural soil, s1R	Local soil, sL
EOL phase – landfill volatilization	Continental air, aC	Regional air, aR	Local air, aL

Table A.4-2 Model input parameters and uncertainty distributions

Model input parameter	Variable name	Units	Base value	SKY_EUR SCENARIO		REF_AMS SCENARIO		UTL_LOC SCENARIO	
				Distribution	Base value	Distribution	Base value	Distribution	Ref.
<i>-- Installation parameters</i>									
Panel conversion efficiency	pv.eff	%	28%	P, $\alpha=25\%$ , $\beta=28\%$ , c=31%	28%	P, $\alpha=25\%$ , c=31%	28%	P, $\alpha=25\%$ , $\beta=28\%$ , c=31%	82
Panel lifetime	LT	years	30	N, $\mu=30$ , $\sigma=5$	30	N, $\mu=30$ , $\sigma=5$	30	N, $\mu=30$ , $\sigma=5$	82
Mass of element per m <sup>2</sup> cell: arsenic	Mu.PVare_a	g/m <sup>2</sup>	8.81	U, min=7.93, max=9.69	8.81	U, min=7.93, max=9.69	8.81	U, min=7.93, max=9.69	2
Mass of element per m <sup>2</sup> cell: gallium	Mu.PVare_a	g/m <sup>2</sup>	15.06	U, min=13.55, max=16.57	15.06	U, min=7.93, max=9.69	15.06	U, min=7.93, max=9.69	2
Mass of element per m <sup>2</sup> cell: indium	Mu.PVare_a	g/m <sup>2</sup>	0.02	U, min=0.018, max=0.022	0.02	U, min=7.93, max=9.69	0.02	U, min=7.93, max=9.69	2
<i>-- Demand scenarios</i>									
Initial capacity addition	C0	MW	100	N/A	0.1	N/A	64	N/A	3
Carrying capacity	Cf	MW	4.3e5	N/A	110	N/A	64	N/A	105,110
Yearly growth rate	K	-	11.4%	N/A	20%	N/A	0	N/A	107
Fraction utility vs. rooftop	f.utility	-	75%	P, $\alpha=25\%$ , $\beta=75\%$ , c=90%	0	P, $\alpha=0.1$ , $c=0.2$	78.1%	N/A	108
Fraction utility floating vs. ground	f.float	-	13.3%	P, $\alpha=5\%$ , $\beta=13.3\%$ , c=20%	0	P, $\alpha=5\%$ , $\beta=13.3\%$ , c=20%	100%	N/A	109
Fraction rooftop draining to water vs. soil	f.roofwat	-	50%	P, $\alpha=10\%$ , $\beta=50\%$ , c=90%	50%	P, $\alpha=10\%$ , $\beta=50\%$ , c=90%	50%	P, $\alpha=10\%$ , $\beta=50\%$ , c=90%	4
Collected PV waste for recycling	f.EOL.rec	-	85%	U, min=85%, max=99.9%	85%	U, min=85%, max=99.9%	85%	U, min=85%, max=99.9%	111
Fraction of arsenic recovered for reuse	frecreu	-	95%	U, min=90%, max=99.9%	95%	U, min=90%, max=99.9%	95%	U, min=90%, max=99.9%	118-120

<sup>1</sup> P: PERT, N: Normal, L: Lognormal, U: Uniform, T: Student's T, E: Exponential.<sup>2</sup> Internal calculations from the SITaSol project (<http://sitasol.com>).<sup>3</sup> Assumed prior, see Chapter 6.<sup>4</sup> Assumed prior, see Chapter 6.

Fraction of gallium recovered for reuse	f.rec.reu	-	95%	U, min=90%, max=99.9%	95%	U, min=90%, max=99.9%	95%	U, min=90%, max=99.9%	118-120
Fraction of indium recovered for reuse	f.rec.reu	-	95%	U, min=90%, max=99.9%	95%	U, min=90%, max=99.9%	95%	U, min=90%, max=99.9%	118-120
Fraction not recycled to incinerator	f.EOL.inc	-	50%	P, a=25%, b=50%, c=75%	100%	N/A	100%	N/A	5
<i>-- Use phase emissions</i>									
Yearly fraction of panels with breakage	f.cracked	-	0.06%	U, min=0% max=0.12%	0.06%	U, min=0.03% max=0.12%	0.06%	U, min=0.03% max=0.12%	121
Number of cracks per panel	n.ncr	5	U, min=1 max=10	5	U, min=1 max=10	5	U, min=1 max=10	5	U, min=1 max=10
Average width of crack	W.cr	mm	1	U, min=0.01 max=1	1	U, min=0.01 max=1	1	U, min=0.01 max=1	67
Average length of crack	L.cr	cm	10	P, a=1, b=10, c=30	10	P, a=1, b=10, c=30	10	P, a=1, b=10, c=30	
Average hours of rain per year	t.train	h	840	P, a=240, b=840, c=1080	840	P, a=240, b=840, c=1080	840	P, a=240, b=840, c=1080	122
Diffusion coefficient of arsenic	D	m <sup>2</sup> /s	1.2e-9	P, a=5e-10, b=1.2e-9, c=1.9e-9	1.2E-9	P, a=5e-10, b=1.2e-9, c=1.9e-9	1.2E-9	P, a=5e-10, b=1.2e-9, c=1.9e-9	123
Diffusion coefficient of gallium	D	m <sup>2</sup> /s	7.9e-10	P, a=6e-10, b=7.9e-10, c=1.9e-9	7.9e-10	P, a=6e-10, b=7.9e-10, c=1.9e-9	7.9e-10	P, a=6e-10, b=7.9e-10, c=1.9e-9	124
Diffusion coefficient of indium	D	m <sup>2</sup> /s	9.8e-10	P, a=6e-10, b=9.8e-10, c=1.9e-9	9.8e-10	P, a=6e-10, b=9.8e-10, c=1.9e-9	9.8e-10	P, a=6e-10, b=9.8e-10, c=1.9e-9	124
Thickness boundary layer of diffusion	d	mm	0.01	U, min=0.01 max=0.1	0.1	U, min=0.1 max=1	0.1	U, min=0.1 max=1	67
Frac. rooftop drainage removed at WTP	f.roof.wtp	-	99%	U, min=98%, max=99.9%	99%	U, min=98%, max=99.9%	99%	U, min=98%, max=99.9%	125
<i>-- EOI phase emissions: landfill</i>									
Landfill cell depth	lfd	m	2.9	E, λ=0.35	2.9	E, λ=0.35	2.9	E, λ=0.35	113
PV waste density (compacted)	wastedens	kg/L	1.38	P, a=1, b=1.38, c=2	1.38	P, a=1, b=1.38, c=2	1.38	P, a=1, b=1.38, c=2	
Fraction of arsenic volatilized in landfill	f.fl.fair	-	6.5%	U, min=2% max=10%	6.5%	U, min=2% max=10%	6.5%	U, min=2% max=10%	116
Effective infiltration through landfill	If.inf	m/yr	0.07	P, a=0, b=0.07, c=0.14	0.07	P, a=0, b=0.07, c=0.14	0.07	P, a=0, b=0.07, c=0.14	113

<sup>5</sup> Assumed prior, see Chapter 6.

Waste/leachate partition coefficient: As	K <sub>w</sub>	L/kg	205	L, $\mu=205, \sigma=4.5$	205	L, $\mu=205, \sigma=4.5$	205	L, $\mu=205, \sigma=4.5$	6
Waste/leachate partition coefficient: Ga	K <sub>w</sub>	L/kg	1,346	L, $\mu=1,346, \sigma=6.4$	1,346	L, $\mu=1,346, \sigma=6.4$	1,346	L, $\mu=1,346, \sigma=6.4$	
Waste/leachate partition coefficient: In	K <sub>w</sub>	L/kg	516	L, $\mu=2,800, \sigma=2.9$	516	L, $\mu=2,800, \sigma=2.9$	516	L, $\mu=2,800, \sigma=2.9$	
-- <i>EOL phase emissions: incineration</i>									
Fraction of arsenic volatilized incinerator	f <sub>inc.esp</sub>	-	50%	U, min=20%, max=80%	50%	U, min=20%, max=80%	50%	U, min=20%, max=80%	126
Fraction of gallium volatilized incinerator	f <sub>inc.esp</sub>	-	0%	None	0%	None	0%	None	117
Fraction of indium volatilized incinerator	f <sub>inc.esp</sub>	-	0%	None	0%	None	0%	None	117
ESP removal of volatilized arsenic	f <sub>esp.lf</sub>	-	99%	U, min=98%, max=99.99%	99%	U, min=98%, max=99.99%	99%	U, min=98%, max=99.99%	126
Fraction of incinerator ash to reuse	f <sub>inc.reu</sub>	-	54%	P, a=25%, b=54%, c=75%	54%	P, a=0.25, b=0.54, c=0.75	54%	P, a=0.25, b=0.54, c=0.75	127
-- <i>Substance parameters</i>									
Solid/water partitioning coefficient: As	K <sub>p</sub> soil	L/kg	750	L, $\mu=750, \sigma=4.5$	750	L, $\mu=750, \sigma=4.5$	750	L, $\mu=750, \sigma=4.5$	128
Solid/water partitioning coefficient: Ga	K <sub>p</sub> soil	L/kg	11,000	L, $\mu=11,000, \sigma=6.4$	11,000	L, $\mu=11,000, \sigma=6.4$	11,000	L, $\mu=11,000, \sigma=6.4$	128
Solid/water partitioning coefficient: In	K <sub>p</sub> soil	L/kg	2,800	L, $\mu=2,800, \sigma=2.9$	2,800	L, $\mu=2,800, \sigma=2.9$	2,800	L, $\mu=2,800, \sigma=2.9$	128
-- <i>Environmental fate: SimpleBox landscape &amp; other parameters</i>									
Area of landscape covered by land	AREAland.	m <sup>2</sup>	3.7E12	N/A	2.2E8	N/A	1.6E7	N/A	129
Area of landscape covered by sea	AREAsea.	m <sup>2</sup>	3.7E12	N/A	0	N/A	N/A	N/A	129

<sup>6</sup> Waste/leachate partitioning coefficients were calculated from the regression equation derived by Allison & Allison<sup>115</sup>:  $\log K_w = 0.7 \log K_{p\text{soil}} + 0.3$ . The relation has a low correlation coefficient ( $R^2 = 0.4$ ) and the obtained values "must be regarded as highly uncertain". To preserve correlations between  $K_w$  and  $K_{p\text{soil}}$ , the  $K_{p\text{soil}}$  (solid/water partitioning coefficient) values used in this formula in every model iteration were the same as those used in the SimpleBox fate model (see "Substance parameters" section in this Table).

Fraction of area freshwater	FRACfresh	-	0.03	N/A	0.24	N/A	0.08	N/A	129
Fraction of area natural soil	FRACnats oil.	-	0.27	N/A	0	N/A	0	N/A	129
Fraction of area agricultural soil	FRACagso il.	-	0.60	N/A	0.18	N/A	0	N/A	129
Fraction of area other soil	FRACothe rsoil.	-	0.70	N/A	0.58	N/A	0	N/A	129
Fraction of soil (local scale)	FRACsoil	-		N/A		N/A	0.92	N/A	129
Temperature	TEMP	°C	12	T, mix=10, mode=12, max=35	12	T, mix=10, mode=12, max=35	12	T, mix=10, mode=12, max=35	130
Average wind speed	WINDspee d	m/s	4.65	PERT, a=0, b=5.1, c=18	4.65	PERT, a=0, b=5.1, c=18	4.65	PERT, a=0, b=5.1, c=18	130
Mixed height air compartment	HEIGHT.a	m	605	T, min=77, mode=400, max=1338	605	T, min=77, mode=400, max=1338	605	T, min=77, mode=400, max=1338	130
Average rainfall	RAINrate	mm/ yr	925	PERT, a=350, b=700, c=2400	925	PERT, a=350, b=700, c=2400	925	PERT, a=350, b=700, c=2400	130
Average depth freshwater compartments	DEPTHfре shwater	m	4.7	PERT, a=1, b=3, c=15	2.6	PERT, a=1, b=3, c=5	4.7	PERT, a=1, b=3, c=15	130
Mixed depth of freshwater sediment	DEPTH.sd	cm	4.7	T, min=1, mode=3, max=10	4.7	T, min=1, mode=3, max=10	4.7	T, min=1, mode=3, max=10	130
Mixed depth of marine sediment	DEPTH.sd	cm	4.7	T, min=1, mode=3, max=10	N/A	N/A	N/A	N/A	130
Volume fraction water in soil	FRACw.s	-	0.29	T, min=0.003, mode=0.2, max=0.67		T, min=0.003, mode=0.2, max=0.67		T, min=0.003, mode=0.2, max=0.67	130
Volume fraction water in sediment	FRACw.sd	-	0.77	T, min=0.5, mode=0.8, max=0.999		T, min=0.5, mode=0.8, max=0.999		T, min=0.5, mode=0.8, max=0.999	130
Mass fraction organic carbon in suspended matter freshwater	CORG.sus p1	-	0.1	L, $\mu=0.1, \sigma=0.04$	0.1	L, $\mu=0.1, \sigma=0.04$	0.1	L, $\mu=0.1, \sigma=0.04$	130
Concentration suspended matter in freshwater	SUSP.w1	mg/L	24.4	L, $\mu=24.4, \sigma=23.5$	24.4	L, $\mu=24.4, \sigma=23.5$	24.4	L, $\mu=24.4, \sigma=23.5$	130

Mass fraction organic carbon in suspended matter seawater	CORG.sus p2	-	0.1	L, $\mu=0.1, \sigma=0.04$	N/A	N/A	N/A	N/A	N/A	130
Concentration suspended matter in seawater	SUSP.w2	mg/L	24.4	L, $\mu=24.4, \sigma=23.5$	N/A	N/A	N/A	N/A	N/A	130
Mass fraction organic carbon in freshwater sediment	CORG.sd1	-	0.05	L, $\mu=0.05, \sigma=0.04$	0.05	L, $\mu=0.05, \sigma=0.04$	0.05	L, $\mu=0.05, \sigma=0.04$	0.05	130
Mass fraction organic carbon in sediment seawater	CORG.sd2	-	0.05	L, $\mu=0.05, \sigma=0.04$	N/A	N/A	N/A	N/A	N/A	130
Mass fraction organic carbon in soil	CORG.s	-	0.05	L, $\mu=0.05, \sigma=0.04$	0.05	L, $\mu=0.05, \sigma=0.04$	0.05	L, $\mu=0.05, \sigma=0.04$	0.05	130
Deposition velocity aerosol particles	AEROSOL deprecate	m/s	1.0E-3	L, $\mu=1.0E-3, \sigma=1.0E-3$	1.0E-3	L, $\mu=1E-3, \sigma=1.0E-3$	1.0E-3	L, $\mu=1.0E-3, \sigma=1.0E-3$	1.0E-3	130
Aerosol collection efficiency	COLLECT eff	-	2.0E4	T, $\min=5.0E3, \max=3.5E4$ , mode=2.0E4,	2.0E4	T, $\min=5.0E3, \max=3.5E4$ , mode=2.0E4,	2.0E4	T, $\min=5.0E3, \max=3.5E4$ , mode=2.0E4,	2.0E4	130
Settling velocity suspended particles	SETLvel octy	m/s	2.1E-5	T, $\min=3.0E-6, \max=3.0E-5$ , mode=2.9E-5,	2.1E-5	T, $\min=3.0E-6, \max=3.0E-5$ , mode=2.9E-5,	2.1E-5	T, $\min=3.0E-6, \max=3.0E-5$ , mode=2.9E-5,	2.1E-5	130
Autochthonous production of suspended matter in freshwater	PRODssusp .w1	g/m <sup>2</sup> /yr	12	T, $\min=5, \max=20$ , mode=10,	12	T, $\min=5, \max=20$ , mode=10,	12	T, $\min=5, \max=20$ , mode=10,	12	130
Autochthonous production of suspended matter in seawater	PRODssusp .w2	g/m <sup>2</sup> /yr	1.2	T, $\min=0.5, \max=2.0$ , mode=1.0,	N/A	N/A	N/A	N/A	N/A	130
Partial mass transfer coefficient water side of water/sediment interface	Kwsch.wate r:w	m/s	4.0E-6	T, $\min=2.78E-6, \max=2.78E-6*3$ , mode=2.78E-6,	4.0E-6	T, $\min=2.78E-6, \max=2.78E-6*3$ , mode=2.78E-6,	4.0E-6	T, $\min=2.78E-6, \max=2.78E-6*3$ , mode=2.78E-6,	4.0E-6	130
Partial mass transfer coefficient sediment side of water/sediment interface	Kwsdsed. sd	m/s	4.0E-8	T, $\min=2.78E-8/3, \max=2.78E-8*3$ , mode=2.78E-8,	4.0E-8	T, $\min=2.78E-8/3, \max=2.78E-8*3$ , mode=2.78E-8,	4.0E-8	T, $\min=2.78E-8/3, \max=2.78E-8*3$ , mode=2.78E-8,	4.0E-8	130
Erosion of soil	EROSION.	mm/s	0.03	T, $\min=0, \max=0.06$ , mode=0.03,	0.03	T, $\min=0, \max=0.06$ , mode=0.03,	0.03	T, $\min=0, \max=0.06$ , mode=0.03,	0.03	130

Volume fraction of precipitation on soil running off to surface water	FRACrn.s	-	0.25	T, min=0, mode=0.25, max=0.50	0.25	T, min=0, mode=0.25, max=0.50	0.25	T, min=0, mode=0.25, max=0.50	130
Volume fraction of precipitation infiltrating into soil	FRACnf.s	-	0.25	T, min=0, mode=0.25, max=0.50	0.25	T, min=0, mode=0.25, max=0.50	0.25	T, min=0, mode=0.25, max=0.50	130
Mineral density sediment and soil	RHOsolid <sub>3</sub>	Kg/m <sup>3</sup>	2.5E3	T, min=2.0E3, mode=2.5E3, max=3.0E3	2.5E3	T, min=2.0E3, mode=2.5E3, max=3.0E3	2.5E3	T, min=2.0E3, mode=2.5E3, max=3.0E3	130

## References

1. García-Valverde, R., Cherni, J. A. & Urbina, A. Life cycle analysis of organic photovoltaic technologies. *Prog. Photovoltaics Res. Appl.* **18**, 535–558 (2010).
2. Ito, M., Komoto, K. & Kurokawa, K. Life-cycle analyses of very-large scale PV systems using six types of PV modules. *Curr. Appl. Phys.* **10**, S271–S273 (2010).
3. Reijnders, L. Design issues for improved environmental performance of dye-sensitized and organic nanoparticulate solar cells. *J. Clean. Prod.* **18**, 307–312 (2010).
4. Bravi, M., Parisi, M. L., Tiezzi, E. & Basosi, R. Life cycle assessment of a micromorph photovoltaic system. *Energy* **36**, 4297–4306 (2011).
5. Espinosa, N., Garcia-Valverde, R. & Krebs, F. C. Life-cycle analysis of product integrated polymer solar cells. *Energy Environ. Sci.* **4**, 1547 (2011).
6. Fthenakis, V. M. & Kim, H. C. Photovoltaics: Life-cycle analyses. *Sol. Energy* **85**, 1609–1628 (2011).
7. Held, M. & Ilg, R. Update of environmental indicators and energy payback time of CdTe PV systems in Europe. *Prog. Photovoltaics Res. Appl.* **19**, 614–626 (2011).
8. Kim, H. C. & Fthenakis, V. M. Comparative life-cycle energy payback analysis of multi-junction a-SiGe and nanocrystalline/a-Si modules. *Prog. Photovoltaics Res. Appl.* **19**, 228–239 (2011).
9. Espinosa, N., García-Valverde, R. & Urbina, A. A life cycle analysis of polymer solar cell modules prepared using roll-to-roll methods under ambient conditions. *Sol. Energy Mater. Sol. Cells* **95**, 1293–1302 (2011).
10. Şengül, H. & Theis, T. L. An environmental impact assessment of quantum dot photovoltaics (QDPV) from raw material acquisition through use. *J. Clean. Prod.* **19**, 21–31 (2011).
11. van der Meulen, R. & Alsema, E. Life-cycle greenhouse gas effects of introducing nano-crystalline materials in thin-film silicon solar cells. *Prog. Photovoltaics Res. Appl.* **19**, 453–463 (2011).
12. Emmott, C. J. M., Urbina, A. & Nelson, J. Environmental and economic assessment of ITO-free electrodes for organic solar cells. *Sol. Energy Mater. Sol. Cells* **97**, 14–21 (2012).
13. Espinosa, N., Hösel, M., Angmo, D. & Krebs, F. C. Solar cells with one-day energy payback for the factories of the future. *Energy Environ. Sci.* **5**, 5117–5132 (2012).
14. Fthenakis, V. Sustainability metrics for extending thin-film photovoltaics to terawatt levels. *MRS Bull.* **37**, 425–430 (2012).
15. Kim, H. C., Fthenakis, V., Choi, J.-K. & Turney, D. E. Life Cycle Greenhouse Gas Emissions of Thin-film Photovoltaic Electricity Generation. *J. Ind. Ecol.* **16**, S110–S121 (2012).

16. Espinosa, N. *et al.* Life cycle assessment of ITO-free flexible polymer solar cells prepared by roll-to-roll coating and printing. *Sol. Energy Mater. Sol. Cells* **97**, 3–13 (2012).
17. Raugei, M., Isasa, M. & Fullana Palmer, P. Potential Cd emissions from end-of-life CdTe PV. *Int. J. Life Cycle Assess.* **17**, 192–198 (2012).
18. Yue, D., Khatav, P., You, F. & Darling, S. B. Deciphering the uncertainties in life cycle energy and environmental analysis of organic photovoltaics. *Energy Environ. Sci.* **5**, 9163 (2012).
19. Zuser, A. & Rechberger, H. Considerations of resource availability in technology development strategies: The case study of photovoltaics. *Resour. Conserv. Recycl.* **56**, 56–65 (2011).
20. Eisenberg, D. A., Yu, M., Lam, C. W., Ogunseitan, O. A. & Schoenung, J. M. Comparative alternative materials assessment to screen toxicity hazards in the life cycle of CIGS thin film photovoltaics. *J. Hazard. Mater.* **260**, 534–542 (2013).
21. Espinosa, N. *et al.* OPV for mobile applications: an evaluation of roll-to-roll processed indium and silver free polymer solar cells through analysis of life cycle, cost and layer quality using inline optical and functional inspection tools. *J. Mater. Chem. A* **1**, 7037 (2013).
22. Fthenakis, V. & Anctil, A. Direct Te mining: Resource availability and impact on cumulative energy demand of CdTe PV life cycles. in *2012 IEEE 38th Photovoltaic Specialists Conference (PVSC) PART 2* 1–6 (IEEE, 2012). doi:10.1109/PVSC-Vol2.2012.6656725.
23. Kim, H. C. & Fthenakis, V. Life Cycle Energy and Climate Change Implications of Nanotechnologies. *J. Ind. Ecol.* **17**, 528–541 (2013).
24. Mohr, N. J., Meijer, A., Huijbregts, M. A. J. & Reijnders, L. Environmental life cycle assessment of roof-integrated flexible amorphous silicon/nanocrystalline silicon solar cell laminate. *Progress in Photovoltaics: Research and Applications* (2013) doi:10.1002/pip.2157.
25. Parisi, M., Maranghi, S., Sinicropi, A. & Basosi, R. Development Of Dye Sensitized Solar Cells: A Life Cycle Perspective For The Environmental And Market Potential Assessment Of A Renewable Energy Technology. *Int. J. Heat Technol.* **31**, 143–148 (2013).
26. Collier, J., Wu, S. & Apul, D. Life cycle environmental impacts from CZTS (copper zinc tin sulfide) and Zn<sub>3</sub>P<sub>2</sub> (zinc phosphide) thin film PV (photovoltaic) cells. *Energy* **74**, 314–321 (2014).
27. Espinosa, N. & Krebs, F. C. Life cycle analysis of organic tandem solar cells: When are they warranted? *Sol. Energy Mater. Sol. Cells* **120**, 692–700 (2014).
28. Espinosa, N., Hösel, M., Jørgensen, M. & Krebs, F. C. Large scale deployment of polymer solar cells on land, on sea and in the air. *Energy Environ. Sci.* **7**, 855 (2014).

29. Kim, H., Cha, K., Fthenakis, V. M., Sinha, P. & Hur, T. Life cycle assessment of cadmium telluride photovoltaic (CdTe PV) systems. *Sol. Energy* **103**, 78–88 (2014).
30. Mann, S. A., de Wild-Scholten, M. J., Fthenakis, V. M., van Sark, W. G. J. H. M. & Sinke, W. C. The energy payback time of advanced crystalline silicon PV modules in 2020: a prospective study. *Prog. Photovoltaics Res. Appl.* **22**, 1180–1194 (2014).
31. Parisi, M. L., Maranghi, S. & Basosi, R. The evolution of the dye sensitized solar cells from Grätzel prototype to up-scaled solar applications: A life cycle assessment approach. *Renew. Sustain. Energy Rev.* **39**, 124–138 (2014).
32. Wender, B. A. *et al.* Illustrating anticipatory life cycle assessment for emerging photovoltaic technologies. *Environ. Sci. Technol.* **48**, 10531–10538 (2014).
33. Espinosa, N., Laurent, A. & Krebs, F. C. Ecodesign of organic photovoltaic modules from Danish and Chinese perspectives. *Energy Environ. Sci.* **8**, 2537–2550 (2015).
34. Fabini, D. Quantifying the Potential for Lead Pollution from Halide Perovskite Photovoltaics. *J. Phys. Chem. Lett.* **6**, 3546–3548 (2015).
35. Gong, J., Darling, S. B. & You, F. Perovskite photovoltaics: life-cycle assessment of energy and environmental impacts. *Energy Environ. Sci.* **8**, 1953–1968 (2015).
36. Louwen, A., van Sark, W. G. J. H. M., Schropp, R. E. I., Turkenburg, W. C. & Faaij, A. P. C. Life-cycle greenhouse gas emissions and energy payback time of current and prospective silicon heterojunction solar cell designs. *Prog. Photovoltaics Res. Appl.* **23**, 1406–1428 (2015).
37. Espinosa, N., Serrano-Luján, L., Urbina, A. & Krebs, F. C. Solution and vapour deposited lead perovskite solar cells: Ecotoxicity from a life cycle assessment perspective. *Sol. Energy Mater. Sol. Cells* **137**, 303–310 (2015).
38. Prado-Lopez, V. *et al.* Tradeoff Evaluation Improves Comparative Life Cycle Assessment: A Photovoltaic Case Study. *J. Ind. Ecol.* **20**, 710–718 (2016).
39. Scott, R. P. & Cullen, A. C. Reducing the life cycle environmental impacts of kesterite solar photovoltaics: comparing carbon and molybdenum back contact options. *Int. J. Life Cycle Assess.* **21**, 29–43 (2016).
40. Serrano-Lujan, L. *et al.* Tin- and Lead-Based Perovskite Solar Cells under Scrutiny: An Environmental Perspective. *Adv. Energy Mater.* **5**, 1501119 (2015).
41. Wetzel, T. & Borchers, S. Update of energy payback time and greenhouse gas emission data for crystalline silicon photovoltaic modules. *Prog. Photovoltaics Res. Appl.* **23**, 1429–1435 (2015).
42. Zhang, J., Gao, X., Deng, Y., Li, B. & Yuan, C. Life Cycle Assessment of Titania Perovskite Solar Cell Technology for Sustainable Design and Manufacturing. *ChemSusChem* **8**, 3882–3891 (2015).
43. Babayigit, A., Ethirajan, A., Muller, M. & Conings, B. Toxicity of organometal halide perovskite solar cells. *Nat. Mater.* **15**, 247 (2016).

44. Bergesen, J. D. & Suh, S. A framework for technological learning in the supply chain: A case study on CdTe photovoltaics. *Appl. Energy* **169**, 721–728 (2016).
45. Celik, I. *et al.* Life Cycle Assessment (LCA) of perovskite PV cells projected from lab to fab. *Solar Energy Materials and Solar Cells* vol. 156 157–169 (2015).
46. Chatzisideris, M. D. & Laurent, A. Ecodesign perspectives of thin-film photovoltaic technologies: A review of life cycle assessment studies. *Sol. Energy Mater. Sol. Cells* **156**, 2–10 (2016).
47. Hengevoss, D., Baumgartner, C., Nisato, G. & Hugi, C. Life Cycle Assessment and eco-efficiency of prospective, flexible, tandem organic photovoltaic module. *Sol. Energy* **137**, 317–327 (2016).
48. Kim, J., Rivera, J. L., Meng, T. Y., Laratte, B. & Chen, S. Review of life cycle assessment of nanomaterials in photovoltaics. *Sol. Energy* **133**, 249–258 (2016).
49. Leccisi, E., Raugei, M. & Fthenakis, V. The Energy and Environmental Performance of Ground-Mounted Photovoltaic Systems—A Timely Update. *Energies* **9**, 622 (2016).
50. Scott, R. P., Cullen, A. C., Fox-Lent, C. & Linkov, I. Can Carbon Nanomaterials Improve CZTS Photovoltaic Devices? Evaluation of Performance and Impacts Using Integrated Life-Cycle Assessment and Decision Analysis. *Risk Anal.* **36**, 1916–1935 (2016).
51. Tsang, M. P., Sonnemann, G. W. & Bassani, D. M. A comparative human health, ecotoxicity, and product environmental assessment on the production of organic and silicon solar cells. *Prog. Photovoltaics Res. Appl.* **24**, 645–655 (2016).
52. Tsang, M. P., Sonnemann, G. W. & Bassani, D. M. Life-cycle assessment of cradle-to-grave opportunities and environmental impacts of organic photovoltaic solar panels compared to conventional technologies. *Sol. Energy Mater. Sol. Cells* **156**, 37–48 (2016).
53. Celik, I. *et al.* Environmental analysis of perovskites and other relevant solar cell technologies in a tandem configuration. *Energy Environ. Sci.* **10**, 1874–1884 (2017).
54. Celik, I., Mason, B. E., Phillips, A. B., Heben, M. J. & Apul, D. Environmental Impacts from Photovoltaic Solar Cells Made with Single Walled Carbon Nanotubes. *Environ. Sci. Technol.* **51**, 4722–4732 (2017).
55. A. dos Reis Benatto, G., Espinosa, N. & Krebs, F. C. Life-Cycle Assessment of Solar Charger with Integrated Organic Photovoltaics. *Adv. Eng. Mater.* **19**, 1700124 (2017).
56. Hauck, M., Ligthart, T., Schaap, M., Boukris, E. & Brouwer, D. Environmental benefits of reduced electricity use exceed impacts from lead use for perovskite based tandem solar cell. *Renew. Energy* **111**, 906–913 (2017).
57. Itten, R. & Stucki, M. Highly efficient 3rd generation multi-junction solar cells using silicon heterojunction and perovskite tandem: Prospective life cycle environmental impacts. *Energies* **10**, 841 (2017).

58. Khaenson, W., Maneewan, S. & Punlek, C. A comparison of the environmental impact of solar power generation using multicrystalline silicon and thin film of amorphous silicon solar cells: case study in Thailand. *J. Ecol. Eng.* **18**, 1–14 (2017).
59. Monteiro Lunardi, M., Wing Yi Ho-Baillie, A., Alvarez-Gaitan, J. P., Moore, S. & Corkish, R. A life cycle assessment of perovskite/silicon tandem solar cells. *Prog. Photovoltaics Res. Appl.* **25**, 679–695 (2017).
60. Vellini, M., Gambini, M. & Prattella, V. Environmental impacts of PV technology throughout the life cycle: Importance of the end-of-life management for Si-panels and CdTe-panels. *Energy* **138**, 1099–1111 (2017).
61. Zhang, J., Gao, X., Deng, Y., Zha, Y. & Yuan, C. Comparison of life cycle environmental impacts of different perovskite solar cell systems. *Sol. Energy Mater. Sol. Cells* **166**, 9–17 (2017).
62. Alberola-Borràs, J.-A. *et al.* Perovskite Photovoltaic Modules: Life Cycle Assessment of Pre-industrial Production Process. *iScience* **9**, 542–551 (2018).
63. Alberola-Borràs, J.-A. *et al.* Relative impacts of methylammonium lead triiodide perovskite solar cells based on life cycle assessment. *Sol. Energy Mater. Sol. Cells* **179**, 169–177 (2018).
64. Alberola-Borràs, J.-A., Vidal, R. & Mora-Seró, I. Evaluation of multiple cation/anion perovskite solar cells through life cycle assessment. *Sustain. Energy Fuels* **2**, 1600–1609 (2018).
65. Amarakoon, S. *et al.* Life cycle assessment of photovoltaic manufacturing consortium (PVMC) copper indium gallium (di)selenide (CIGS) modules. *Int. J. Life Cycle Assess.* **23**, 851–866 (2018).
66. Celik, I. *et al.* Energy Payback Time (EPBT) and Energy Return on Energy Invested (EROI) of Perovskite Tandem Photovoltaic Solar Cells. *IEEE J. Photovoltaics* **8**, 305–309 (2018).
67. Celik, I., Song, Z., Phillips, A. B., Heben, M. J. & Apul, D. Life cycle analysis of metals in emerging photovoltaic (PV) technologies: A modeling approach to estimate use phase leaching. *J. Clean. Prod.* **186**, 632–639 (2018).
68. Monteiro Lunardi, M. *et al.* A comparative life cycle assessment of chalcogenide/Si tandem solar modules. *Energy* (2018) doi:10.1016/J.ENERGY.2017.12.130.
69. M. Lunardi, M., Alvarez-Gaitan, J. P., Chang, N. L. & Corkish, R. Life cycle assessment on PERC solar modules. *Sol. Energy Mater. Sol. Cells* **187**, 154–159 (2018).
70. Mokhtarimehr, M., Forbes, I. & Pearsall, N. Environmental assessment of vacuum and non-vacuum techniques for the fabrication of Cu<sub>2</sub>ZnSnS<sub>4</sub> thin film photovoltaic cells. *Jpn. J. Appl. Phys.* **57**, 08RC14 (2018).
71. Moore, E. A., Babbitt, C. W., Gaustad, G. & Moore, S. T. Portfolio Optimization of Nanomaterial Use in Clean Energy Technologies. *Environ. Sci. Technol.* **52**, 4440–4448 (2018).

72. Munshi, A. H. *et al.* Thin-film CdTe photovoltaics – The technology for utility scale sustainable energy generation. *Sol. Energy* **173**, 511–516 (2018).
73. Pallas, G., Peijnenburg, W., Guinée, J., Heijungs, R. & Vijver, M. Green and Clean: Reviewing the Justification of Claims for Nanomaterials from a Sustainability Point of View. *Sustainability* **10**, 689 (2018).
74. Ravikumar, D., Seager, T. P., Cucurachi, S., Prado, V. & Mutel, C. Novel Method of Sensitivity Analysis Improves the Prioritization of Research in Anticipatory Life Cycle Assessment of Emerging Technologies. *Environ. Sci. Technol. acs.est.7b04517* (2018) doi:10.1021/acs.est.7b04517.
75. Bani Salim, M., Emre Demirocak, D. & Barakat, N. A Fuzzy Based Model for Standardized Sustainability Assessment of Photovoltaic Cells. *Sustainability* **10**, 4787 (2018).
76. Sinha, P. & Wade, A. Addressing Hotspots in the Product Environmental Footprint of CdTe Photovoltaics. *IEEE J. Photovoltaics* 1–5 (2018) doi:10.1109/JPHOTOV.2018.2802786.
77. Soares, W. M., Athayde, D. D. & Nunes, E. H. M. LCA study of photovoltaic systems based on different technologies. *Int. J. Green Energy* **15**, 577–583 (2018).
78. Stamford, L. & Azapagic, A. Environmental Impacts of Photovoltaics: The Effects of Technological Improvements and Transfer of Manufacturing from Europe to China. *Energy Technol.* **6**, 1148–1160 (2018).
79. Zhou, Z. & Carbajales-Dale, M. Assessing the photovoltaic technology landscape: efficiency and energy return on investment (EROI). *Energy Environ. Sci.* **11**, 603–608 (2018).
80. Billen, P. *et al.* Comparative evaluation of lead emissions and toxicity potential in the life cycle of lead halide perovskite photovoltaics. *Energy* **166**, 1089–1096 (2019).
81. Pallas, G., Vijver, M. G., Peijnenburg, W. J. G. M. & Guinée, J. Life cycle assessment of emerging technologies at the lab scale: The case of nanowire-based solar cells. *J. Ind. Ecol. jiec.12855* (2019) doi:10.1111/jiec.12855.
82. Blanco, C. F. *et al.* Environmental impacts of III–V/silicon photovoltaics: life cycle assessment and guidance for sustainable manufacturing. *Energy Environ. Sci.* **13**, 4280–4290 (2020).
83. Louwen, A., Van Sark, W. G. J. H. M., Schropp, R. E. I., Turkenburg, W. C. & Faaij, A. P. C. Life-cycle greenhouse gas emissions and energy payback time of current and prospective silicon heterojunction solar cell designs. *Progress in Photovoltaics: Research and Applications* vol. 23 1406–1428 (2015).
84. Paschotta, R. Wall-plug efficiency. *RP Photonics Encyclopedia* (2019).
85. Wood, D. *et al.* Passivated Busbars from Screen-printed Low-temperature Copper Paste. *Energy Procedia* **55**, 724–732 (2014).
86. Wernet, G. *et al.* The ecoinvent database version 3 (part I): overview and methodology. *Int. J. Life Cycle Assess.* **21**, 1218–1230 (2016).

87. Spath, P. L. & Mann, M. K. *Life cycle assessment of hydrogen production via natural gas steam reforming*. National Renewable Energy Laboratory (2001).
88. Mehmeti, A., Angelis-Dimakis, A., Arampatzis, G., McPhail, S. & Ulgiati, S. Life Cycle Assessment and Water Footprint of Hydrogen Production Methods: From Conventional to Emerging Technologies. *Environments* **5**, 24 (2018).
89. Cetinkaya, E., Dincer, I. & Naterer, G. F. Life cycle assessment of various hydrogen production methods. *Int. J. Hydrogen Energy* **37**, 2071–2080 (2012).
90. Balaji, R. *et al.* Development and performance evaluation of Proton Exchange Membrane (PEM) based hydrogen generator for portable applications. *Int. J. Hydrogen Energy* **36**, 1399–1403 (2011).
91. Smith, B. L., Babbitt, C. W., Horowitz, K., Gaustad, G. & Hubbard, S. M. Life Cycle Assessment of III-V Precursors for Photovoltaic and Semiconductor Applications. *MRS Adv.* **3**, 1399–1404 (2018).
92. Guerin, J. An increased portfolio for waste gas abatement. *Compound Semiconductors* 18–22 (2016).
93. Hsu, J.-N., Tsai, C.-J., Chiang, C. & Li, S.-N. Silane Removal at Ambient Temperature by Using Alumina-Supported Metal Oxide Adsorbents. *J. Air Waste Manage. Assoc.* **57**, 204–210 (2007).
94. Pacaud, B., Popa, J.-M. & Cartier, C.-B. Purification of silane gas. (1990).
95. CS Clean Systems. Safety Data Sheet - Cleansorb CS3C. (2014).
96. Wang, X. *et al.* Arsine adsorption in copper-exchanged zeolite under low temperature and micro-oxygen conditions. *RSC Adv.* **7**, 56638–56647 (2017).
97. Li, W.-C. *et al.* Metal Loaded Zeolite Adsorbents for Phosphine Removal. *Ind. Eng. Chem. Res.* **47**, 1501–1505 (2008).
98. Heitmann, U. *et al.* Novel Approach for the Bonding of III-V on Silicon Tandem Solar Cells with a Transparent Conductive Adhesive. in *2018 IEEE 7th World Conference on Photovoltaic Energy Conversion, WCPEC 2018 - A Joint Conference of 45th IEEE PVSC, 28th PVSEC and 34th EU PVSEC* 201–205 (IEEE, 2018). doi:10.1109/PVSC.2018.8548276.
99. Chaudhuri, M. K. *et al.* Process for making metal acetylacetones. (2002).
100. Matovu, J. B., Ong, P., Leunissen, L. H. A., Krishnan, S. & Babu, S. V. Fundamental Investigation of Chemical Mechanical Polishing of GaAs in Silica Dispersions: Material Removal and Arsenic Trihydride Formation Pathways. *ECS J. Solid State Sci. Technol.* **2**, P432–P439 (2013).
101. Heijungs, R. & Suh, S. *The Computational Structure of Life Cycle Assessment*. vol. 11 (Springer Netherlands, 2002).
102. Borgonovo, E. A new uncertainty importance measure. *Reliab. Eng. Syst. Saf.* **92**, 771–784 (2007).

103. Borgonovo, E. & Iooss, B. Moment-Independent and Reliability-Based Importance Measures. in *Handbook of Uncertainty Quantification* (eds. Ghanem, R., Higdon, D. & Owhadi, H.) 1265–1287 (Springer International Publishing, 2017). doi:10.1007/978-3-319-11259-6\_37-1.
104. Henriksson, P. J. G. *et al.* Product carbon footprints and their uncertainties in comparative decision contexts. *PLoS One* **10**, 1–11 (2015).
105. Shell International B.V. Sky Scenario. *Shell Scenarios SKY Meeting the Goals of the Paris Agreement* <https://www.shell.com/energy-and-innovation/the-energy-future/scenarios/shell-scenario-sky.html> (2018).
106. Global Solar Atlas. <https://globalsolaratlas.info/map?c=50.958427,15.512695,4&s=47.338823,5.976563&m=site>.
107. Jaxa-Rozen, M. & Trutnevyyte, E. Sources of uncertainty in long-term global scenarios of solar photovoltaic technology. *Nat. Clim. Chang.* **11**, 266–273 (2021).
108. IEA. *The Role of Critical Minerals in Clean Energy Transitions*. (2021).
109. Cazzaniga, R. & Rosa-Clot, M. The booming of floating PV. *Sol. Energy* **219**, 3–10 (2021).
110. City of Amsterdam. Policy: Renewable energy. *Policy: Sustainability and energy* <https://www.amsterdam.nl/en/policy/sustainability/renewable-energy/>.
111. European Parliament; Council of the European Union. *Directive 2012/19/EU of the European Parliament and of the Council of 4 July 2012 on waste electrical and electronic equipment (WEEE)*. (2012). doi:10.3000/19770677.L\_2012.197.eng.
112. Mathai, A. M., Moschopoulos, P. & Pederzoli, G. Random points associated with rectangles. *Rend. del Circ. Mat. di Palermo* **48**, 163–190 (1999).
113. U.S. Environmental Protection Agency Office of Solid Waste. *EPA's Composite Model for Leachate Migration with Transformation Products (EPACMTP) Parameters/Data Background Document*. [https://www.epa.gov/smm/epas-composite-model-leachate-migration-transformation-products-epacmtp#:~:text=Related%20Topics%3A-,EPA's%20Composite%20Model%20for%20Leachate%20Migration%20with%20Transformation%20Products%20\(EPACMTP\),constituents%20to%20the%20subsurface%20environment](https://www.epa.gov/smm/epas-composite-model-leachate-migration-transformation-products-epacmtp#:~:text=Related%20Topics%3A-,EPA's%20Composite%20Model%20for%20Leachate%20Migration%20with%20Transformation%20Products%20(EPACMTP),constituents%20to%20the%20subsurface%20environment). (2003).
114. U.S. Environmental Protection Agency Office of Solid Waste. *EPA's Composite Model for Leachate Migration with Transformation Products (EPACMTP) Technical Background Document*. (2003).
115. Allison, J. D. & Allison, T. L. *Partitioning Coefficients for Metals in Surface Water, Soil and Waste*. [https://cfpub.epa.gov/si/si\\_public\\_record\\_report.cfm?Lab=NERL&dirEntryId=135783](https://cfpub.epa.gov/si/si_public_record_report.cfm?Lab=NERL&dirEntryId=135783) (2005).
116. Webster, T. M. *et al.* Anaerobic Disposal of Arsenic-Bearing Wastes Results in Low Microbially Mediated Arsenic Volatilization. *Environ. Sci. Technol.* **50**, 10951–10959 (2016).

117. Uryu, T., Yoshinaga, J. & Yanagisawa, Y. Environmental Fate of Gallium Arsenide Semiconductor Disposal. *J. Ind. Ecol.* **7**, 103–112 (2003).
118. Zhan, L., Wang, Z., Zhang, Y. & Xu, Z. Recycling of metals (Ga, In, As and Ag) from waste light-emitting diodes in sub/supercritical ethanol. *Resour. Conserv. Recycl.* **155**, (2020).
119. Van Den Bossche, A., Vereycken, W., Vander Hoogerstraete, T., Dehaen, W. & Binnemans, K. Recovery of Gallium, Indium, and Arsenic from Semiconductors Using Tribromide Ionic Liquids. *ACS Sustain. Chem. Eng.* **7**, 14451–14459 (2019).
120. Zhan, L., Xia, F., Xia, Y. & Xie, B. Recycle Gallium and Arsenic from GaAs-Based E-Wastes via Pyrolysis-Vacuum Metallurgy Separation: Theory and Feasibility. *ACS Sustain. Chem. Eng.* **6**, 1336–1342 (2018).
121. Köntges, M. *et al.* *Review of Failures of Photovoltaic Modules.* [https://iea-pvps.org/wp-content/uploads/2020/01/IEA-PVPS\\_T13-01\\_2014\\_Review\\_of\\_Failures\\_of\\_Photovoltaic\\_Modules\\_Final.pdf](https://iea-pvps.org/wp-content/uploads/2020/01/IEA-PVPS_T13-01_2014_Review_of_Failures_of_Photovoltaic_Modules_Final.pdf) (2014).
122. Hosseinzadehtalaei, P., Tabari, H. & Willems, P. Climate change impact on short-duration extreme precipitation and intensity–duration–frequency curves over Europe. *J. Hydrol.* **590**, 125249 (2020).
123. Tanaka, M. *et al.* The difference of diffusion coefficients in water for arsenic compounds at various pH and its dominant factors implied by molecular simulations. *Geochim. Cosmochim. Acta* **105**, 360–371 (2013).
124. Vanýsek, P. Ionic conductivity and diffusion at infinite dilution. in *Handbook of Chemistry and Physics* (5-111)-(5-113) (CRC Press, 1992).
125. Sun, L., Lu, M., Li, Q., Jiang, H. & Yin, S. Research progress of arsenic removal from wastewater. *IOP Conf. Ser. Earth Environ. Sci.* **218**, 012142 (2019).
126. Jung, C. ., Matsuto, T., Tanaka, N. & Okada, T. Metal distribution in incineration residues of municipal solid waste (MSW) in Japan. *Waste Manag.* **24**, 381–391 (2004).
127. Blasenbauer, D. *et al.* Legal situation and current practice of waste incineration bottom ash utilisation in Europe. *Waste Manag.* **102**, 868–883 (2020).
128. Sheppard, M. I., Sheppard, S. C. & Grant, C. A. Solid/liquid partition coefficients to model trace element critical loads for agricultural soils in Canada. *Can. J. Soil Sci.* **87**, 189–201 (2007).
129. Vermeire, T. G. *et al.* European Union System for the Evaluation of Substances (EUSES). Principles and structure. *Chemosphere* **34**, 1823–1836 (1997).
130. Bakker, J., Brandes, L. J., den Hollander, H. A., van de Meent, D. & Struijs, J. *Validating SimpleBox-Computed Steady-state Concentration Ratios.* (2003).